Optimal Placement and Validation of PV Inverter with Voltage Control Capability in Active Distribution Systems

by

Mengxi Chen

A Dissertation Presented in Partial Fulfillment
of the Requirements for the Degree
Doctor of Philosophy

Approved April 2023 by the
Graduate Supervisory Committee:

Vijay Vittal, Co-Chair
Raja Ayyanar, Co-Chair
Mojdeh Khorsand
Meng Wu

ARIZONA STATE UNIVERSITY

May 2023

ABSTRACT

The high R/X ratio of typical distribution systems makes the system voltage vulnerable to active power injection from the distributed energy resources (DERs). Moreover, the intermittent and uncertain nature of the DER generation brings new challenges to voltage management. As guided by the previous IEEE standard 1547-2003, most of the existing photovoltaic (PV) systems in the real distribution networks are equipped with conventional inverters, which only allow the PV systems to operate at unity power factor to generate active power. To utilize the voltage control capability of the existing PV systems following the guideline of the revised IEEE standard 1547-2018, this dissertation proposes a two-stage stochastic optimization strategy aimed at optimally placing the PV smart inverters with Volt-VAr capability among the existing PV systems for distribution systems with high PV penetration to mitigate voltage violations.

PV smart inverters are fast-response devices compared to conventional voltage control devices in the distribution system. Historically, distribution system planning and operation studies are mainly based on quasi-static simulation, which ignores system dynamic transitions between static solutions. However, as high-penetration PV systems are present in the distribution system, the fast transients of the PV smart inverters cannot be ignored. A detailed dynamic model of the PV smart inverter with Volt-VAr control capability is developed as a dynamic link library (DLL) in OpenDSS to validate the system voltage stability with autonomous control of the optimally placed PV smart inverters. Static and dynamic verification is conducted on an actual 12.47 kV, 9 km-long Arizona utility feeder that serves residential customers.

To achieve fast simulation and accommodate more complex PV models with desired accuracy and efficiency, an integrative dynamic simulation framework for OpenDSS with adaptive step size control is proposed. Based on the original fixed-step

size simulation framework in OpenDSS, the proposed framework adds a function in the OpenDSS main program to adjust its step size to meet the minimum step size requirement from all the PV inverters in the system. Simulations are conducted using both the original and the proposed framework to validate the proposed simulation framework.

ACKNOWLEDGMENTS

I would like to thank my co-advisors Dr. Vijay Vittal and Dr. Raja Ayyanar for offering me this opportunity to pursue a doctoral degree in power engineering at Arizona State University. Their continuous support and profound knowledge in this field of expertise have always been encouraging and inspiring me during my entire Ph.D. life.

I'm also grateful to my committee members, Dr. Mojdeh Khorsand and Dr. Meng Wu, for their insightful advice on my research work. I would like to thank Dr. Shanshan Ma, who is a post-doctoral researcher and gave me a lot of valuable advice and help on the project we are working on. Her self-motivated research spirit and high execution have always impressed me.

Additionally, I would like to thank Douglas Welsh, James Cronen, and Shruti Dwarkanath Rao, who offered me the opportunity of an internship in the PSLF software team of General Electric (GE). I learned the relationship between my research work and industrial practice during my internship in the team and I got a better idea of how I should contribute my efforts to the industrial practice after my graduation.

Last, I want to thank my parents who have been supporting me both emotionally and financially after I left my home country for higher education.

TABLE OF CONTENTS

CHAPTER Page

LIST OF TABLES

LIST OF FIGURES

Figure Page

NOMENCLATURE

φ	Set of phase indices p
$\varphi(\ell)$	Subset of phase at distribution line ℓ
$\Omega_{\mathcal{B}}$	Set of bus indices (i, p)
$\Omega_{\mathcal{D}} \subset \Omega_{\mathcal{B}}$	Subset of bus with load indices (d, p)
$\Omega_{\mathcal{L}}$	Set of distribution lines indices (ℓ, p)
$\mathcal{L}_O(i)$	Subset of distribution lines (ℓ, p) originating at bus i
$\mathcal{L}_E(i)$	Subset of distribution lines (ℓ, p) ending at bus i
ℓ_o, ℓ_e	From-node and to-node indices of distribution line ℓ
$\Omega_{\mathcal{PV}} \subset \Omega_{\mathcal{B}}$	Subset of bus with PV indices (g, p)
$\Omega_{\mathcal{PV}_{vv}} \subset \Omega_{\mathcal{PV}}$	Subset of bus with PV candidates for smart inverters indices (g, p)
Ω_{TR}	Set of transformers indices (r, p)
Ω_{sub}	Set of substation indice (n, p)
$\mathcal{S}$	Set of scenarios indices s
c_a^{pv}	Allocation cost of the PV smart inverter
c_p^{pv}	PV active power curtailment cost
$R_{\ell,p,m}$	Self resistance $(p = m)$ and mutual resistance of line ℓ between phases p and m $(p \neq m)$
$X_{\ell,p,m}$	Self reactance $(p = m)$ and mutual reactance of line ℓ between phases p and m $(p \neq m)$

$Z_{\ell,p,m}$	Self impedance ($p = m$) and mutual impedance of line ℓ between phases p and m ($p \neq m$)
$y_{\ell,m,k}$	Susceptance of line ℓ between phases m and k
$\bar{P}_{g,p}^{pv,s}$	The maximum power point (MPP) of PV at bus g phase p at scenario s
$\bar{P}_{g,p}^{pv,\max}$	The rating active power value of PV inverter at bus g phase p
$\bar{Q}_{g,p}^{pv,\max}$	The rating reactive power value of PV inverter at bus g phase p
$\bar{S}_{g,p}^{pv}$	The rating apparent power value of PV inverter at bus g phase p
$\bar{V}_g^{(1)}, \ldots, \bar{V}_g^{(6)}$	Voltage magnitude breakpoints of the linear piece-wise Q-V curve
$V^{\min}/V^{\max}$	The minimum/maximum voltage magnitude for the normal operation
$\bar{V}_{n,p}^{r,s}/\bar{V}_{n,p}^{im,s}$	Real/imaginary part of voltage measurement at substation before enabling Volt-VAr control n phase p at scenario s
$p_r(s)$	The scenario probability
w_c, w_o^s, w_v^s	The weight coefficients in the objective function
$P_{n,p}^{G,s}$	Injection from substation n at phase p at scenario s
$P_{r,p}^{Tr,s}$	No-load loss of transformer r at phase p at scenario s
$P_{d,p}^{D,s}$	Active power of load at bus d phase p at scenario s
$Q_{d,p}^{D,s}$	Active power of load at bus d phase p at scenario s
M	A large positive number
$PF_{\min}$	The minimum power factor of PV smart inverter

$x_{g,p}^{pv}$	Binary variable to decide whether to place an PV smart inverter or not at bus g phase p
$x_{g,p}^{pv_{on},s}$	Binary variable to enable PV Volt-VAr control function at bus g phase p at scenario s
$x_{g,p}^{pv_{off},s}$	Binary variable to disable PV Volt-VAr control function at bus g phase p scenario s
$P_{g,p}^{pv,s}$	Active power output of PV at bus g phase p at scenario s
$Q_{g,p}^{pv,s}$	Reactive power output of PV at bus g phase p at scenario s
$Q_{g,p}^{qv,s}$	Reactive power output of PV following Q-V curve at bus g phase p at scenario s
$I_{\ell,p}^{r,s}$	Real part of current flow at line ℓ phase p at scenario s
$I_{\ell,p}^{im,s}$	Imaginary part of current flow at line ℓ phase p at scenario s
$I_{i,p}^{in,r,s}$	Real part of current injection at bus i phase p at scenario s
$I_{i,p}^{in,im,s}$	Imaginary part of current injection at bus i phase p at scenario s
$V_{i,p}^{r,s}$	Real part of voltage at bus i phase p at scenario s
$V_{i,p}^{im,s}$	Imaginary part of voltage at bus i phase p at scenario s
$V_{i,p}^{m,s}$	Voltage magnitude at bus i phase p at scenario s
$\phi(x^{pv}, s)$	Operation cost of the second stage at scenario s given $x_{g,p}^{pv}$

Chapter 1

INTRODUCTION

1.1 Motivation

The rapid growth of distributed energy resources (DERs), especially solar photovoltaic (PV) generators in distribution systems, is changing systems from passive networks to active ones [1]. The large R/X ratio of the active distribution feeders makes the voltages sensitive to the intermittent active power injection from the PVs, which may lead to unexpected voltage violations and voltage fluctuations [2]. This evolution introduces new voltage management challenges to both the distribution system planner and operator [3].

Following the guideline of the new IEEE standard for interconnection and interoperability of DERs [4], PVs with smart inverters can control and optimize local voltage by injecting or absorbing reactive power based on the local voltage. However, PV technologies had been evolving for many years with the previous IEEE 1547-2003 standard [5] requiring that the DERs not to actively regulate the voltage at the point of common coupling (PCC) before the new standard [4] was published. Most of the existing PVs in the distribution systems are still equipped with conventional inverters that can only generate active power. Retrofitting all or a huge number of existing inverters in the system to have reactive power support capability can be cost-prohibitive. So it is necessary to develop a decision-making tool with an optimal planning strategy to selectively upgrade the existing conventional PV inverters, which can mitigate the system-wide voltage violation issues in various real-time operating conditions with minimal costs.

On the other hand, in order to verify the effectiveness and stability of the optimally upgraded PV smart inverters in the distribution system, it is necessary to simulate the system with the optimally placed smart inverters in both static and dynamic modes using a reliable distribution simulator. OpenDSS is one of the commonly used distribution system simulators, which has been widely applied in static and quasi-static time series (QSTS) power flow analysis. The static and quasi-static simulations are sufficient for analyzing distribution system control and switching operation due to the power variation from the load and the limited amount of inverter-based resources (IBRs) in the past [6]. In this work, a detailed dynamic model of the PV smart inverter with Volt-VAr control capability is needed to test the dynamic impact of the optimally placed PV smart inverters on the distribution system in OpenDSS. However, OpenDSS does not provide an embedded dynamic PV inverter model, and hence, users need to develop their own sophisticated model in a dynamic link library (DLL) as needed for dynamic simulations.

OpenDSS has an embedded predictor–corrector method with a fixed step size framework for dynamic simulation with phasors. With the embedded simulation framework, the whole system including the distribution network and the external dynamic model in OpenDSS needs to be simulated using a fixed-time step which has to be small enough to keep the simulation numerically stable. This step size could be unnecessarily small when the system reaches a stable state and results in a long simulation time. Moreover, OpenDSS only works with phasors, while power electronic devices like PV inverters are usually modeled in conventional electromagnetic transient (EMT) simulation tools, which deal with natural signal waveforms in the time domain.

PV inverter models with linear control functions can be easily transformed from the time-domain model to the phasor-domain model using dynamic phasor trans-

formation because linear models can be represented using single-frequency phasors. However, harmonic signals with various frequencies could be generated in nonlinear models, and as a result, single-frequency phasors are not sufficient to represent the nonlinear model dynamics. It is necessary to represent all the frequency components that dominate the model dynamics in phasor-domain models, however, it is difficult to capture a broad spectrum of the model transients with a limited amount of frequency components considered. In such cases, the simulation of transient waveforms (i.e., time-domain EMT model) is required to capture all the necessary dynamics[7]. To accommodate the time-domain model in OpenDSS simulation, a hybrid model should be developed in the DLL that can both do the time-domain simulation and exchange data between the time-domain model and the phasor-domain network in OpenDSS using a proper phasor extraction technique.

To achieve faster dynamic simulation and accommodate more complex PV dynamic models with desired numerical stability and efficiency, the fixed-step size dynamic simulation framework for OpenDSS needs to be improved. This allows the distribution system modeled in OpenDSS and PV smart inverters modeled in the DLL to be simulated at the same variable step size. Compared to the original fixed-step size simulation framework, the improved framework can significantly increase the simulation efficiency while keeping the simulation numerically stable.

1.2 Voltage Control Strategies in Active Distribution System

1.2.1 Voltage management in the operational stage

To manage the voltage challenges due to the increased penetration level of DERs, there are several kinds of voltage control strategies that have been applied in the operation of active distribution systems: local control, distributed control, decentralized

control, and centralized control [8].

- The local control is an autonomous control strategy that does not require any communication among different controllers [9; 10; 11; 12]. For example, the Volt-VAr and Volt-Watt controllers can utilize the local voltage and current measurements to regulate the voltage at the point-of-connection (PoC) by providing active and reactive power support. In [12], the authors proposed a proportional Volt-VAr-Watt control strategy where the setting of the controllers can be updated by solving a robust optimization problem. This method can quickly adapt to the changing local operating conditions but cannot fully utilize the controller capability due to a lack of communication.

- The centralized control can provide more flexibility by allowing the optimal utilization of the control devices among the entire system. However, a robust communication system is required to provide the real-time measurements for the central controller [13; 14; 15]. In [16], two voltage control algorithms were combined together, one using specific control rules to determine the actions of different control devices and the other optimizing the coordinated operation using a centralized strategy.

- The distributed and decentralized control strategies are two other options for voltage management. Both require less communication among different devices and can provide more robust solutions than the centralized method.

  Distributed control is a strategy that does not need a central controller; only the communication between the neighboring controllers is required [17]. The decentralized control coordinates various control components to optimize the operation for a specific area, which means the system can be divided into different "centralized" zones [18].

These different control strategies are all based on the voltage regulation devices that already exist in the system and only focus on the system operation stage with possible use of optimization techniques to coordinate the operation of different devices. However, the existing control devices in some distribution systems may not be adequate for handling the voltage issues caused by the increasing penetration of PVs. Even worse, the bidirectional power flow of the active distribution network can mislead traditional control devices such as tap changers and cause unexpected regulating or protecting actions [1].

1.2.2 Voltage management in the planning stage

To overcome the voltage management difficulty caused by the high penetration level of PVs with intermittent nature, it is necessary to adopt an effective control strategy in the operational stage and also develop an effective planning strategy that takes active voltage control operation into account. Many approaches in distribution system planning associated with active voltage management have been investigated [19; 20; 21; 22; 23; 24]. The authors in [25] proposed a planning procedure coordinated with a centralized voltage regulation system that considers the voltage control by a combination of the tap changers, capacitor banks, and available reactive power from the DERs. An integrated planning model was developed in [26] to optimally allocate DERs with the coordination of a real-time decentralized control scheme of different voltage control devices to minimize the voltage deviations. Those planning strategies focused on increasing the penetration level of the DERs and optimizing the locations and sizes of the DERs without considering their real-time operational characteristic. The system voltage regulation flexibility is limited by the capability of existing control devices and the communication system.

To further mitigate voltage violation issues in the active distribution system, the

interconnection standard IEEE 1547-2003 has been thoroughly revised and published as 1547-2018 to allow smart inverter-based generators to participate in the distribution feeder voltage regulation by providing sufficient active and reactive power support [4]. This amendment enables the DERs with smart inverters to control and optimize the local voltage by injecting or absorbing reactive power based on the local voltage. For a distribution system with a high penetration level of residential PVs resulting in voltage violation problems, utilizing the local voltage management capability of the smart PV inverter is one of the most cost-effective methods for system planners to regulate voltage. Compared with centralized and decentralized control strategies, which require a certain level of communication, the smart inverter with voltage control capability can use local voltage measurements to manage the system-wide voltage. It can also decrease the operational uncertainty in the planning stage caused by possible communication delays, noises, or failures.

In order to better utilize the local control capability of the PV smart inverters in the distribution system, various optimal Volt-VAr control (VVC) strategies have been studied by the previous research efforts [27; 28; 29; 30; 31; 32]. These articles focus on the operational or short-term planning aspect of the reactive power optimization in multiple timescales such as the day ahead prediction stage, hourly prediction stage, and real-time stage. By using multi-timescale optimization, centrally coordinated control between the PV smart inverters and traditional voltage control devices such as the capacitor banks and the on-load tap changers (OLTC) can be achieved by considering their different response speeds.

Few long-term voltage control planning strategies take the real-time PV inverter operation into consideration. A joint planning and operation optimization algorithm was presented in [33; 34] to upgrade traditional expansion measures and consider the voltage regulation impact of DERs with smart inverters in the operation stage.

However, the inverter Q-V characteristic was discretized and implemented through a look-up table [34], and an iterative procedure was used to ensure voltage and reactive power convergence. They did not implement the actual operational Q-V curves of the smart inverters in the planning process, which is more accurate. Moreover, the authors assumed that the existing inverters should be retrofitted for the desired control characteristics, which is not realistic.

1.3 Dynamic simulation of PV Inverters in Distribution Systems

Electric power grids are undergoing a significant transition in the generation mix with the growing penetration of IBRs [35], such as inverter-based PV and wind generators. Historically, distribution system studies are mainly based on quasi-static simulation, which ignores system dynamic transitions between static solutions [6]. The quasi-static simulation is sufficient for analyzing system control and switching operation due to the power variation from the load and the limited amount of IBRs in the past [6]. However, as more inverter-based PV systems with various control capabilities are being installed in distribution systems, their dynamic impacts can not be ignored. It becomes essential to examine the dynamic interactions between the PV systems and the system to which they are connected. Power electronic devices like PV inverters are usually modeled in conventional electromagnetic transient (EMT) simulation tools, which deal with natural signal waveforms and contain the most accurate detail of the inverter dynamics. It requires the simulation step size to be several microseconds or even less. However, current distribution system simulators like OpenDSS are phasor-based, which ignore the system's electromagnetic transient and allow the system to be simulated with a larger step size, typically milliseconds, to increase efficiency.

Previous research has put great efforts into simulating the dynamic impact of

the increasing penetration of inverter-based PV resources as well as their various control capabilities on large-scale distribution systems. Those research works can be summarized into two categories: (a) Represent the PV inverter EMT model by a phasor domain model and simulate the entire system in the phasor domain; (b) Co-simulate the detailed PV inverter EMT model with the external phasor-based system. The phasor model sacrifices the PV model accuracy by ignoring some high-frequency transients but allows the use of a larger integration step size [36; 37; 38]. Given that no frequency-dependence is represented, the phasor model for the inverter is valid and accurate for most simulation needs in the distribution system [7]. However, as the PV control techniques evolve rapidly, there is a need to implement nonlinear controllers in the PV model. For example, [39][40] applied adaptive nonlinear control to grid-connected PV in the weak distribution grid to accommodate various grid impedances. In such cases, the simulation of transient waveforms (i.e., EMT model) is required to capture all the necessary dynamics[7].

The concept of co-simulation has been applied in the simulation of IBRs in the distribution system and other transient simulations that require both EMT details and faster simulation time in recent years[41; 42; 43; 44; 45; 46]. In the co-simulation framework, detailed EMT models are present only in small parts of the entire system where accurate models are required, the remaining part of the system (external system) is represented in the phasor domain. Interfacing two types of simulation programs always needs them to run at different step sizes, which makes the interaction protocol and the equivalent models of the external and detailed system critical to the simulation accuracy and efficiency. Firstly, the data exchange always happens at the time step of the phasor simulator which is much larger than the EMT simulator step. This will raise the problem in the EMT simulator when it runs at much smaller time steps that information from the phasor simulator is not updated and result in power

flow divergence. Secondly, in the co-simulation framework, both the EMT simulator and phasor simulator require an accurate equivalent model of the external system in the other simulation program to ensure the simulation validity.

1.4 Research Objectives

The objectives of the research work can be described as follows:

- Develop an optimization tool to optimally upgrade the existing PV inverters in a distribution system to smart inverters that have Volt-VAr control capability with minimal allocation and operational costs. The program should take the uncertainties of PV generation and load demand into consideration. The optimally upgraded PV inverters should be able to mitigate the system-wide voltage violations by regulating the local voltage of each upgraded PV inverter.

- Develop a dynamic model for PV inverters with linear control functions and Volt-VAr control capability in a DLL for dynamic simulation in OpenDSS. The model should be able to inject and absorb reactive current to and from the distribution network based on the terminal voltage provided by OpenDSS.

- Develop a dynamic model for PV inverters with nonlinear control function and Volt-VAr control capability in a DLL for dynamic simulation in OpenDSS. The dynamic model should be represented in the time domain instead of the phasor domain and have an appropriate data exchange technique between the time-domain model and the phasor-domain network in OpenDSS.

- Develop an integrative dynamic simulation framework for OpenDSS with adaptive step size control to study the dynamic impact of the PV inverters on the distribution system with desired dynamic simulation accuracy and computational efficiency. The integrative simulation network should be able to adjust

the dynamic simulation step size automatically based on the evaluation of the integration error of each time step within the dynamic model. The integrative simulation framework should be able to ensure the numerical stability of the dynamic simulation while increasing the simulation efficiency compared to the original fixed-time step simulation framework in OpenDSS. Compared to the co-simulation framework, the developed integrative framework can simulate the detailed PV systems and the external system at the same step size simultaneously without an equivalent model. It can eliminate information mismatches caused by the step size mismatch between the detailed systems and the external system.

1.5 Report Organization

The remainder of this report is organized as follows:

Chapter 2 presents a long-term distribution system planning methodology developed for voltage management. A two-stage stochastic mixed-integer linear programming model is developed to determine optimal numbers and locations of PV smart inverters with Volt-VAr control to mitigate under/over voltage conditions while minimizing the active power curtailment of PV units in active distribution networks. Chapter 3 introduces the dynamic simulation in OpenDSS and presents the PV inverter dynamic model with both linear and nonlinear control functions developed for dynamic simulation in OpenDSS. Chapter 4 presents the integrative simulation framework developed for a more accurate and efficient dynamic simulation in OpenDSS.

Chapter 2

OPTIMAL PLACEMENT OF PV SMART INVERTERS WITH VOLT-VAR CONTROL

In this section, a two-stage stochastic mixed-integer linear programming model is developed to determine optimal numbers and locations of PV inverters to be upgraded with Volt-VAr control in a certain distribution system to mitigate under/over voltage conditions while minimizing the active power curtailment of PV units.

2.1 Problem Statement

The increased penetration of PVs in distribution systems may lead to severe voltage violation problems or reactive power problems [47]. PVs with smart inverters can control and optimize the local voltage by injecting or absorbing reactive power based on the local voltage. However, PV technologies have been evolving for many years with the previous IEEE 1547-2003 standard [5] declaring that the DERs shall not actively regulate the voltage at the point of common coupling (PCC) before the new standard [4] was published. Most of the existing PVs in the distribution systems are still equipped with conventional inverters that can only generate active power. Retrofitting all or a large number of existing inverters to have Volt-VAr capability can be cost-prohibitive for the utilities.

On the other hand, to maximize the voltage control capability of smart inverters, especially during periods of peak solar output, the smart inverter may need to operate under VAr priority mode. It indicates that the reactive power support is prioritized, the active power output may need to be curtailed due to the lack of sufficient headroom in the inverter rating. However, curtailing the active power output of PVs

negates the economic benefit to PV owners and other environmental benefits.

A novel long-term planning strategy to place the minimum number of PV smart inverters with Volt-VAr control considering the uncertainties of PV output and load is developed to solve these problems. The problem is formulated as a two-stage stochastic decision process: (i) smart inverter placement decisions for the rooftop PV is made in the first stage (planning stage); (ii) the operational uncertainties are resolved in worst-case voltage conditions considering the load demand and PV output; recourse decisions (i.e., Volt-VAr control) are invoked to minimize voltage violation in the second stage. Uncertainty is constructed using the historical data from a utility by considering two worst voltage scenarios: The worst over-voltage scenario occurs under the maximum PV generation condition; the worst under-voltage scenario considers the maximum load condition.

2.2 Problem Formulation

This section presents the formulation of a two-stage stochastic mixed-integer linear program (SMILP) to place the minimum number of PV smart inverters with Volt-VAr control to meet the voltage requirements and mitigate the voltage violations in under/over-voltage conditions.

2.2.1 First-stage and second-stage objective formulation

The first stage minimizes the number of PV smart inverters. The second stage minimizes the Euclidean norm of PVs' active power curtailment while maintaining the substation voltage at a certain level given the worst voltage scenario. Equation (2.1) presents the objective of the developed SMILP problem, which minimizes the allocation cost of PV smart inverters and the expected operation cost of the second stage.

$$\min \; w_c \sum_{(g,p)\in\Omega_{\mathcal{PV}}} x^{pv}_{g,p} + \sum_{s\in\mathcal{S}} p_r(s)\phi(x^{pv}, s) \tag{2.1}$$

The second stage models the unbalanced distribution system operation under a worst case voltage scenario given the PV smart inverter placement decision from the first stage. There are two modeling challenges. Firstly, it is essential to model the Volt-VAr control with VAR priority analytically. If a PV smart inverter works in the Volt-VAr control mode, the generated reactive power should follow a specific Q-V curve as shown in Fig. 2.1, which varies with its local voltage magnitude. As Fig. 2.1 depicts, once the voltage magnitude drops below the dead-zone, the PV smart inverter operates in the injection mode to generate reactive power to increase its local voltage. The PV smart inverter does not generate any reactive power if the voltage is in the dead-zone range. When the voltage is above the dead-zone, the PV smart inverter operates in the absorption mode to absorb reactive power to decrease its local voltage. This Volt-VAr control function can be analytically achieved using the piece-wise linear Q-V curve constraint. At the same time, the Euclidean norm of active power curtailment is minimized in the objective to encourage more PV smart inverters needed to participate in voltage violation mitigation through reactive power support.

Secondly, a multi-phase optimal power flow formulation that models the unbalanced distribution system accurately is needed to obtain the optimal location of PV smart inverters with Volt-VAr control based on actual system requirements. This program makes full use of the unbalanced distribution system linearized AC power flow formulation developed in [48] to model all details of a distribution network. This linearized power flow model is based on the rectangular Current-Voltage (IV) formulation and uses the first-order approximation of the Taylor's series expansion to linearize the nonlinear product of current and voltage in the node power balance con-

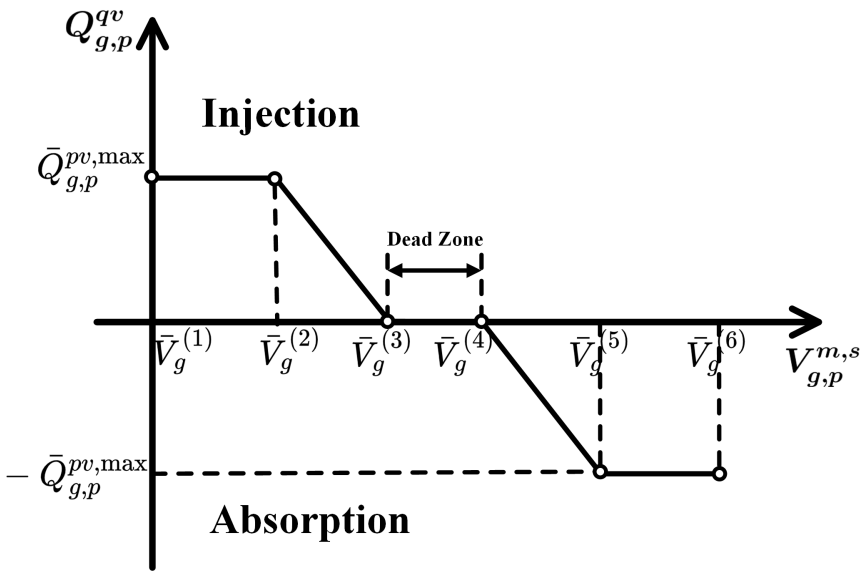

Figure 2.1: Q-V Curve of PV with Volt-VAr Control

straint. In order to construct the Q-V curve constraints for modeling the reactive power of PV smart inverters with Volt-VAr control, the voltage magnitude is needed, which can be obtained using a nonlinear function of real and imaginary parts of voltage in the IV formulation. A similar first-order approximation of the Taylor's series expansion is used to get the linear expression of the voltage magnitude.

The detailed mathematical formulation of the second-stage problem is described as follows:

$$\begin{aligned}\phi(x^{pv}, s) = \min\ & w_o^s \sum_{(g,p)\in\Omega_{\mathcal{PV}}} \left(P_{g,p}^{pv,s} - \bar{P}_{g,p}^{pv,s}\right)^2 \\ & + w_v^s \sum_{(n,p)\in\Omega_{sub}} \left(\left(V_{n,p}^{r,s} - \bar{V}_{n,p}^{r,s}\right)^2 + \left(V_{n,p}^{im,s} - \bar{V}_{n,p}^{im,s}\right)^2\right)\end{aligned} \tag{2.2}$$

The first part of the detailed second-stage formulation in (2.2) minimizes the weighted least squares of the active power curtailment of PV with the smart Volt-VAr control. The second set of terms minimizes the weighted least squares of the feeder-head voltage difference between the optimization model and the base case without PV Volt-VAr control.

2.2.2 Smart inverter Volt-VAr control constraints

PV Volt-VAr control enabling constraint

$$x_{g,p}^{pv_{on}} \leqslant x_{g,p}^{pv}, \forall (g,p) \in \Omega_{\mathcal{PV}_{vv}}, s \in \mathcal{S} \tag{2.3}$$

Constraint (2.3) indicates that only if a PV smart inverter is placed at the selected PV bus node g phase p, the Volt-VAr control function can be enabled; otherwise, it will not be activated. Here $\Omega_{\mathcal{PV}_{vv}}$ is a pool of candidate PVs in the optimization that can be selected to install a PV smart inverter.

PV output disjunctive constraints

$$\begin{bmatrix} x_{g,p}^{pv_{on},s} \\ 0 \leqslant P_{g,p}^{pv,s} \leqslant \bar{P}_{g,p}^{pv,s} \\ Q_{g,p}^{pv,s} = Q_{g,p}^{qv,s} \\ P_{g,p}^{pv,s2} + Q_{g,p}^{pv,s2} \leqslant (\bar{S}_{g,p}^{pv})^2 \end{bmatrix} \bigvee_{\substack{\forall (g,p) \in \Omega_{\mathcal{PV}_{vv}} \\ s \in \mathcal{S}}} \begin{bmatrix} x_{g,p}^{pv_{off},s} \\ P_{g,p}^{pv,s} = \bar{P}_{g,p}^{pv,s} \\ Q_{g,p}^{pv,s} = 0 \end{bmatrix} \tag{2.4}$$

$$x_{g,p}^{pv_{on},s}, x_{g,p}^{pv_{off},s} \in \{\text{True, False}\}, \forall (g,p) \in \Omega_{\mathcal{PV}_{vv}}, s \in \mathcal{S}$$

The disjunction constraint (2.4) describes the logical relationship of the PV output with a binary decision, whether to enable Volt-VAr control function or not. Here $x_{g,p}^{pv_{on},s}$ and $x_{g,p}^{pv_{off},s}$ are used as binary variables to select between different groups of PV output constraints. These binary variables must satisfy the relationship $x_{g,p}^{pv_{on},s} + x_{g,p}^{pv_{off},s} = 1$. If $x_{g,p}^{pv_{on},s} = 1$, it indicates that the PV at bus g can perform Volt-VAr control: the active power output of the PV can be curtailed; the reactive power output of the PV needs to follow the Q-V curve as shown in Fig. 2.1, which varies with the voltage magnitude $V_{g,p}^{m}$; and the apparent power output of PV should be less than the rated apparent power value $\bar{S}_{g,p}^{pv}$. If $x_{g,p}^{pv_{off},s} = 1$, it indicates that the PV at bus g does not perform Volt-VAr control: the active power output of the PV is equal to the maximum power point for the PV, and its reactive power output is zero.

Piecewise-linear Q-V curve constraint

The Q-V curve of Volt-VAr control shown in Fig. 2.1 can be expressed as a continuous piecewise-linear function:

$$Q_{g,p}^{qv,s} = \begin{cases} \bar{Q}_{g,p}^{pv,\max} & \text{if } \bar{V}_g^{(1)} \leqslant V_{g,p}^{m,s} \leqslant \bar{V}_g^{(2)} \\ \frac{\bar{Q}_{g,p}^{pv,\max}}{\bar{V}_g^{(2)} - V_g^{(1)}} \left(\bar{V}_g^{(2)} - V_{g,p}^{m,s} \right) & \text{if } \bar{V}_g^{(2)} \leqslant V_{g,p}^{m,s} \leqslant \bar{V}_g^{(3)} \\ 0 & \text{if } \bar{V}_g^{(3)} \leqslant V_{g,p}^{m,s} \leqslant \bar{V}_g^{(4)} \\ \frac{\bar{Q}_{g,p}^{pv,\max}}{\bar{V}_g^{(3)} - \bar{V}_g^{(4)}} \left(V_{g,p}^{m,s} - \bar{V}_g^{(3)} \right) & \text{if } \bar{V}_g^{(4)} \leqslant V_{g,p}^{m,s} \leqslant \bar{V}_g^{(5)} \\ -\bar{Q}_{g,p}^{pv,\max} & \text{if } \bar{V}_g^{(5)} \leqslant V_{g,p}^{m,s} \leqslant \bar{V}_g^{(6)} \end{cases} \tag{2.5}$$

This piecewise linear function of the Q-V curve is defined by a list of voltage magnitude breakpoints denoted by $\bar{V}_g^j \in \left\{ \bar{V}_g^{(1)}, \bar{V}_g^{(2)}, \ldots, \bar{V}_g^{(6)} \right\}$ and a list of function values (i.e., PV reactive power outputs) corresponding to each voltage magnitude breakpoint. The function value, denoted by $Q_{g,p}^{qv,s}$, among these voltage magnitude breakpoints is implied through linear interpolation. A disaggregated convex combination model is used to transform this function into a block of variables and constraints that enforces a piece-wise linear relationship between the voltage magnitude variable (i.e., $V_{g,p}^{m,s}$) and the PV reactive power output variable (i.e., $Q_{g,p}^{qv,s}$). Let $\bar{Q}_g^j \in \left\{ \bar{Q}_{g,p}^{pv,\max}, \bar{Q}_{g,p}^{pv,\max}, 0, 0, -\bar{Q}_{g,p}^{pv,\max}, -\bar{Q}_{g,p}^{pv,\max} \right\}$ represents the corresponding reactive output at the voltage magnitude breakpoints of the Q-V curve. The reformulated constraints of (2.5) can be written as:

$$V_{g,p}^{m,s} = \sum_{j \in \mathcal{J}} \left(\bar{V}_g^{(j)} \lambda_{g,p}^{j,j,s} + \bar{V}_g^{(j+1)} \lambda_{g,p}^{j,j+1,s} \right), \quad \forall (g,p) \in \Omega_{\mathcal{PV}}, s \in \mathcal{S} \tag{2.6}$$

$$Q_{g,p}^{qv,s} = \sum_{j \in \mathcal{J}} \left(\bar{Q}_g^j \lambda_{g,p}^{j,j,s} + \bar{Q}_g^{j+1} \lambda_{g,p}^{j,j+1,s} \right), \forall (g,p) \in \Omega_{\mathcal{PV}}, s \in \mathcal{S} \tag{2.7}$$

$$\delta_{g,p}^{j,s} = \lambda_{g,p}^{j,j,s} + \lambda_{g,p}^{j,j+1,s}, \forall (g,p) \in \Omega_{\mathcal{PV}}, j \in \mathcal{J}, s \in \mathcal{S} \tag{2.8}$$

$$\sum_{j\in\mathcal{J}} \delta_{g,p}^{j,s} = 1, \forall(g,p) \in \Omega_{\mathcal{PV}}, s \in \mathcal{S} \tag{2.9}$$

$$\delta_{g,p}^{j,s} \in \{0,1\}, \forall(g,p) \in \Omega_{\mathcal{PV}}, j \in \mathcal{J}, s \in \mathcal{S} \tag{2.10}$$

$$\lambda_{g,p}^{j,k,s} \geqslant 0, \forall(g,p) \in \Omega_{\mathcal{PV}}, (j,k) \in \mathcal{K}, s \in \mathcal{S} \tag{2.11}$$

where $\mathcal{J}$ is the set of line segments of the Q-V curve, and $|\mathcal{J}|$ is equal to 5. $\delta_{g,p}^{j,s}$ represents the binary variable selection of line segment j. $\lambda_{g}^{j,k,s}, \forall(j,k) \in \mathcal{K}$ is defined as a weight variable to perform the interpolation on the selected segment j, where k represents the two end points belonging to line segment j and $\mathcal{K}$ is the mapping set of the connecting line segment and its corresponding end-point. $\bar{V}_g^{(2)}, \bar{V}_g^{(3)}, \bar{V}_g^{(4)}$, and $\bar{V}_g^{(5)}$ are the setpoints for the Q-V control curve, which can be adjusted in a specific allowable range. The maximum reactive power of the PV with the Volt-VAr control in (2.5) can be assumed to be the following:

$$\bar{Q}_{g,p}^{pv,max} = \sqrt{\left(\frac{1}{PF_{\min}{}^2} - 1\right)} \bar{P}_{g,p}^{pv,max}, \forall(g,p) \in \Omega_{\mathcal{PV}_w} \tag{2.12}$$

where $PF_{\min}$ represents the minimum power factor that the inverter is capable of operating at rated active power and $P_{g,p}^{pv,max}$ is the maximum active power output of the g-th PV source among all the time-series values given in the data. Based on (2.12), the PV's apparent power rating in (2.4) can be assumed to be:

$$\bar{S}_{g,p}^{pv} = \sqrt{\bar{Q}_{g,p}^{pv,\max 2} + \bar{P}_{g,p}^{pv,\max 2}}, \forall(g,p) \in \Omega_{\mathcal{PV}_w} \tag{2.13}$$

2.2.3 Linearized IV-based AC Power Flow Constraints

The objective of mitigating voltage violations under the worst voltage scenarios with the minimum number of PV smart inverters with Volt-VAr control makes the placement decisions very sensitive to the voltage change. As a result, it is necessary to accurately model the three-phase unbalanced distribution system power flow considering the impact of lines' mutual impedances and shunt admittances on the bus

voltage. Compared with the widely-used linearized DistFlow model, which approximates the unbalanced voltage as balanced [49; 50], the IV-based AC power flow model developed in [48] has been validated to be more accurate to capture the operation characteristics of the unbalanced distribution systems with a high penetration level of PVs.

Line flow constraints

$$\begin{aligned} V^{r,s}_{\ell_o,p} - V^{r,s}_{\ell_e,p} = \sum_{m\in\varphi(\ell)} R_{\ell,p,m}\left(I^{r,s}_{\ell,m} + \sum_{k\in\varphi(\ell)} y_{\ell,m,k}V^{im,s}_{\ell_o,k}\right) \\ - \sum_{m\in\varphi(\ell)} X_{\ell,p,m}\left(I^{im,s}_{\ell,m} - \sum_{k\in\varphi(\ell)} y_{\ell,m,k}V^{r,s}_{\ell_o,k}\right), \forall(\ell,p)\in\Omega_{\mathcal{L}}, s\in\mathcal{S} \end{aligned} \tag{2.14}$$

$$\begin{aligned} V^{im,s}_{\ell_o,p} - V^{im,s}_{\ell_e,p} = \sum_{m\in\varphi(\ell)} R_{\ell,p,m}\left(I^{im,s}_{\ell,m} + \sum_{k\in\varphi(\ell)} y_{\ell,m,k}V^{r,s}_{\ell_o,k}\right) \\ - \sum_{m\in\varphi(\ell)} X_{\ell,p,m}\left(I^{r,s}_{\ell,m} - \sum_{k\in\varphi(\ell)} y_{\ell,m,k}V^{im,s}_{\ell_o,k}\right), \forall(\ell,p)\in\Omega_{\mathcal{L}}, s\in\mathcal{S} \end{aligned} \tag{2.15}$$

Constraints (2.14)-(2.15) describe the relationship of line current and corresponding bus voltage difference over a distribution line connecting bus ℓ_o to bus ℓ_e considering the impact of the line's self and mutual impedances and admittances.

Current injection constraints

$$I^{in,r,s}_{i,p} = \sum_{(\ell,p)\epsilon\mathcal{L}_O(i)} I^{r,s}_{\ell,p} - \sum_{(\ell,p)\epsilon\mathcal{L}_E(i)} I^{r,s}_{\ell,p}, \forall(i,p)\in\Omega_{\mathcal{B}}, s\in\mathcal{S} \tag{2.16}$$

$$I^{in,im,s}_{i,p} = \sum_{(\ell,p)\epsilon\mathcal{L}_O(i)} I^{im,s}_{\ell,p} - \sum_{(\ell,p)\epsilon\mathcal{L}_E(i)} I^{im,s}_{\ell,p}, \forall(i,p)\in\Omega_{\mathcal{B}}, s\in\mathcal{S} \tag{2.17}$$

The injected current at each node and scenario is obtained using (2.16)-(2.17).

Linearized power balance constraints

In the rectangular IV formulation, the power balance constraints contain nonlinear elements due to the product of voltage and injected current. To linearize the power

balance constraints, an iterative first-order approximation of the Taylor's series expansion developed in [48] is used and the linearized power balance constraints around an operating point for each phase (i.e., $\hat{V}_{i,p}^{r,s}, \hat{V}_{i,p}^{im,s}, \hat{I}_{i,p}^{in,r,s}$, and $\hat{I}_{i,p}^{in,im,s}$) can be expressed as (2.18) and (2.19):

$$\begin{aligned}
&\sum_{\substack{\forall(n,p)\in\Omega_{sub}\\ n=i}} P_{n,p}^{G,s} + \sum_{\substack{\forall(g,p)\in\Omega_{\mathcal{PV}_{vv}}\\ g=i}} P_{g,p}^{pv,s} + \sum_{\substack{\forall(g,p)\in\Omega_{\mathcal{PV}_{wo}}\\ g=i}} \bar{P}_{g,p}^{pv,s} - \sum_{\substack{\forall(d,p)\in\Omega_{\mathcal{D}}\\ d=i}} P_{d,p}^{D,s} \\
&- \sum_{\substack{\forall(m,p)\in\Omega_{TR}\\ m=i}} P_{m,p}^{Tr,s} = \hat{V}_{i,p}^{r,s} I_{i,p}^{in,r,s} + \hat{I}_{i,p}^{in,r,s} V_{i,p}^{r,s} + \hat{V}_{i,p}^{im,s} I_{i,p}^{in,im,s} \\
&+ \hat{I}_{i,p}^{in,im,s} V_{i,p}^{im,s} - \hat{V}_{i,p}^{r,s} \hat{I}_{i,p}^{in,r,s} - \hat{V}_{i,p}^{im,s} \hat{I}_{i,p}^{in,im,s}, \forall(i,p)\in\Omega_{\mathcal{B}}, s\in\mathcal{S}
\end{aligned} \tag{2.18}$$

$$\begin{aligned}
&\sum_{\substack{\forall(n,p)\in\Omega_{sub}\\ n=i}} Q_{n,p}^{G,s} + \sum_{\substack{\forall(g,p)\in\Omega_{\mathcal{PV}_{vv}}\\ g=i}} Q_{g,p}^{pv,s} - \sum_{\substack{\forall(d,p)\in\Omega_{\mathcal{D}}\\ d=i}} Q_{d,p}^{D,s} = \hat{V}_{i,p}^{im,s} I_{i,p}^{in,r,s} \\
&- \hat{V}_{i,p}^{r,s} I_{i,p}^{in,im,s} + \hat{I}_{i,p}^{in,r,s} V_{i,p}^{im,s} - \hat{I}_{i,p}^{in,im,s} V_{i,p}^{r,s} - \hat{V}_{i,p}^{im,s} \hat{I}_{i,p}^{in,r,s} \\
&- \hat{V}_{i,p}^{r,s} \hat{I}_{i,p}^{in,im,s}, \forall(i,p)\in\Omega_{\mathcal{B}}, s\in\mathcal{S}
\end{aligned} \tag{2.19}$$

Two PV operating conditions are considered in the developed SMILP problem (i) without smart inverter and (ii) with smart inverter. Since the objective of this placement problem is to minimize the number of PV smart inverters to mitigate the voltage violations in the worst-case scenarios, the PV operating condition without placing smart inverters here is considered to be the base case. In constraints (2.18)-(2.19), $(\hat{V}_{i,p}^{r,s}, \hat{V}_{i,p}^{im,s}, \hat{I}_{i,p}^{in,r,s}, \hat{I}_{i,p}^{in,im,s})$ are the real and imaginary parts of bus voltage and injected current at the operating point without smart inverter, which are used as the first-order approximation parameters of Taylor's series expansion and can be updated iteratively for getting the voltage and injected current at the operating point with smart inverter. Note in constraint (2.18), the active power output of the residential PVs that are not in the PV smart inverter candidate pool is assumed to follow the respective maximum power point (MPP) value.

Voltage magnitude constraints

The voltage magnitude can be expressed by a nonlinear function of the real part and the imaginary part of voltage in (2.20).

$$V_{i,p}^{m,s} = \sqrt{V_{i,p}^{r,s2} + V_{i,p}^{im,s2}}, \forall (i,p) \in \Omega_{\mathcal{B}}, s \in \mathcal{S} \tag{2.20}$$

The linear approximation of (2.20) can be reformulated by the similar first-order Taylor-series expansion method:

$$\begin{aligned} V_{i,p}^{m,s} = & \sqrt{\hat{V}_{i,p}^{r,s2} + \hat{V}_{i,p}^{im,s2}} + \left.\frac{\partial V_{i,p}^{m,s}}{\partial V_{i,p}^{r,s}}\right|_{\hat{V}_{i,p}^{r,s}} (V_{i,p}^{r,s} - \hat{V}_{i,p}^{r,s}) \\ & + \left.\frac{\partial V_{i,p}^{m,s}}{\partial V_{i,p}^{im,s}}\right|_{\hat{V}_{i,p}^{im,s}} (V_{i,p}^{im,s} - \hat{V}_{i,p}^{im,s}) \\ = & \frac{\hat{V}_{i,p}^{r,s} V_{i,p}^{r,s}}{\sqrt{\hat{V}_{i,p}^{r,s2} + \hat{V}_{i,p}^{im,s2}}} + \frac{\hat{V}_{i,p}^{im,s} V_{i,p}^{im,s}}{\sqrt{\hat{V}_{i,p}^{r,s2} + \hat{V}_{i,p}^{im,s2}}} \end{aligned} \tag{2.21}$$

where $(\hat{V}_{i,p}^{r,s}, \hat{V}_{i,p}^{im,s})$ represent the operating point without smart inverter for the first iteration of Taylor's series expansion at bus i, phase p, and scenario s. Constraint (2.22) bounds the voltage magnitudes in the normal operating range.

$$V^{\min} \leqslant V_{i,p}^{m,s} \leqslant V^{\max}, \forall (i,p) \in \Omega_{\mathcal{B}}, s \in \mathcal{S} \tag{2.22}$$

2.3 Test System and Scenario Generation

The two-stage SMILP is tested on an actual 12.47 kV, 9 km-long Arizona utility feeder that serves residential customers. This feeder has 7864 buses, 1790 primary sections, 5782 secondary sections, 371 distribution transformers, 1737 loads, and 766 residential rooftop PV units. These 766 residential rooftop PV units only operate at unity power factor following the maximum power point tracking (MPPT) to generate active power, which results in overvoltages during spring days when excessive power is generated with light load conditions. However, when PV generation is not enough

to cover the heavy load consumption in the summer days, there are undervoltage issues.

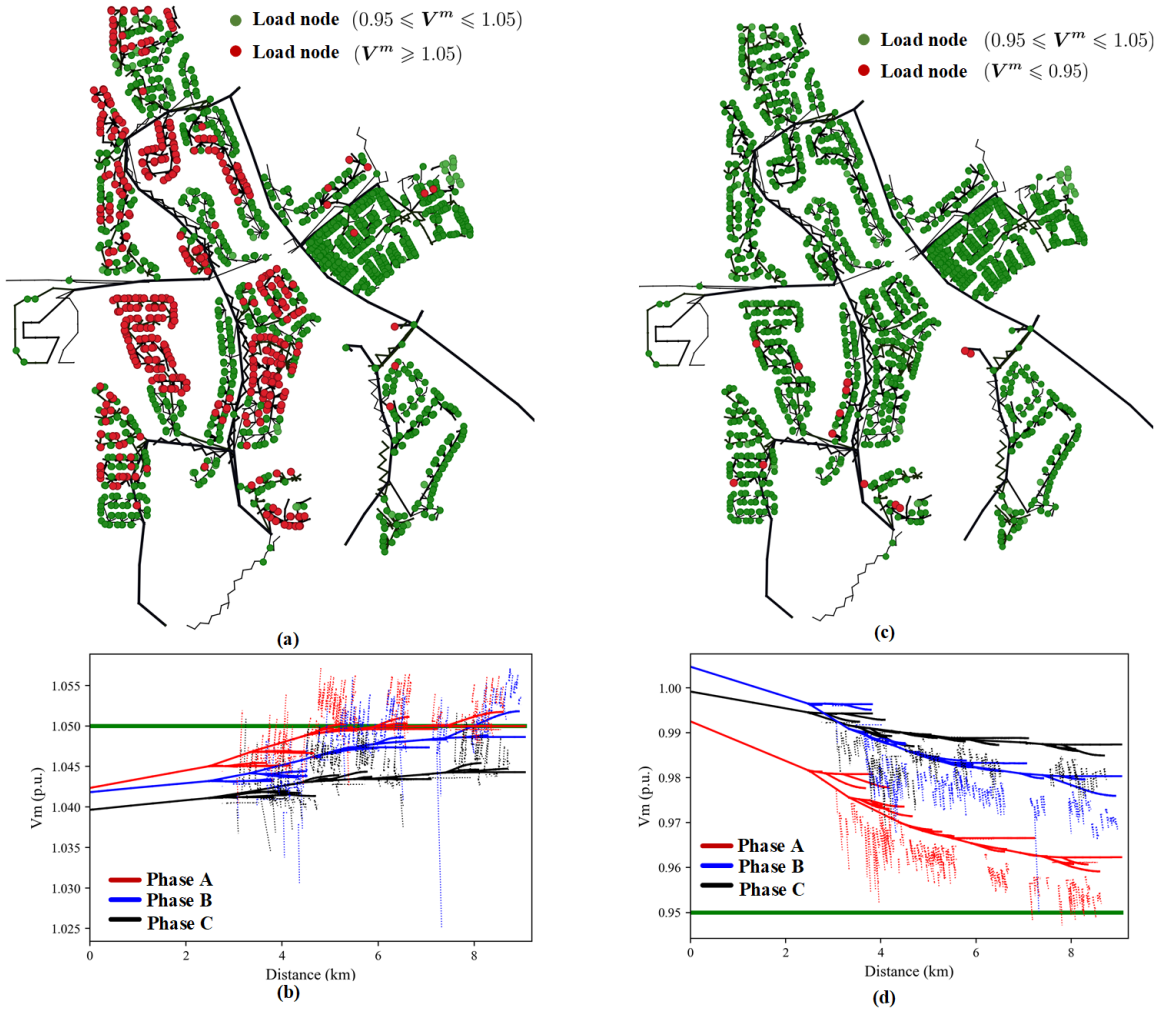

Figure 2.2: Feeder Voltage Violation Maps and Feeder Voltage Profiles in Over- and Under-Voltage Scenarios

Two days corresponding to the actual historical feeder data - the maximum generation condition on 03/15/2019 (high PV) and load peak on 07/15/2019 (high load and relatively low PV) were chosen for constructing the worst over and under voltage scenarios. In the worst over-voltage scenario, the power generated by the installed residential rooftop PV is 3.6MW, which corresponds to a penetration level of 225% (3.6MW/1.6MW) compared to the feeder's corresponding total gross load. Fig. 2.2

(a) presents the load node locations with the over-voltage issue, and the total number of over-voltage load nodes is 439. The voltage profile of the worst over-voltage scenario in the OpenDSS simulation is shown in Fig. 2.2 (b). In the worst under-voltage scenario, Fig. 2.2 (c) presents the load node locations with the under-voltage issue, and the total number of under-voltage load nodes is 14. Fig. 2.2 (d) shows the voltage profile of the worst under-voltage scenario in the OpenDSS simulation.

2.4 Simulation Results and Validation

2.4.1 Optimal placement of PV smart inverters

The set points of the smart inverters are set as shown in Table. 2.1:

Table 2.1: PV Smart Inverter Default Set Points

Parameter	$\bar{\boldsymbol{V}}_{\boldsymbol{g}}^{(\mathbf{1})}$	$\bar{\boldsymbol{V}}_{\boldsymbol{g}}^{(\mathbf{2})}$	$\bar{\boldsymbol{V}}_{\boldsymbol{g}}^{(\mathbf{3})}$	$\bar{\boldsymbol{V}}_{\boldsymbol{g}}^{(\mathbf{4})}$	$\bar{\boldsymbol{V}}_{\boldsymbol{g}}^{(\mathbf{5})}$	$\bar{\boldsymbol{V}}_{\boldsymbol{g}}^{(\mathbf{6})}$
Value	0.0	0.94	0.98	1.02	1.06	1.1

The power factor range of PV smart inverters is $[-0.8, 0.8]$. The optimal location of the PV smart inverters given by the developed SMIP model is shown in Fig. 2.3 and the total number is 99. There are 8 PV smart inverters in Phase A, 69 in Phase B, and 22 in Phase C. OpenDSS is a commonly used distribution system simulator for static and quasi-static time-series (QSTS) power flow analysis. The selected PV smart inverters with Volt-VAr control are implemented in OpenDSS to validate the accuracy and effectiveness of the developed SMIP model. By comparing Fig. 2.2 (a) and Fig. 2.3, it can be seen that the optimization typically favors the locations with overvoltages initially for the placement of smart inverters. The voltage profiles after enabling the optimally selected Volt-VAr control in the OpenDSS simulation under the two worst voltage scenarios are shown in Fig. 2.4. It can be seen that the

optimally placed PV smart inverters with Volt-VAr control can successfully mitigate the voltage violation issues for both over-voltage and under-voltage scenarios, which validates the effectiveness of the SMIP model.

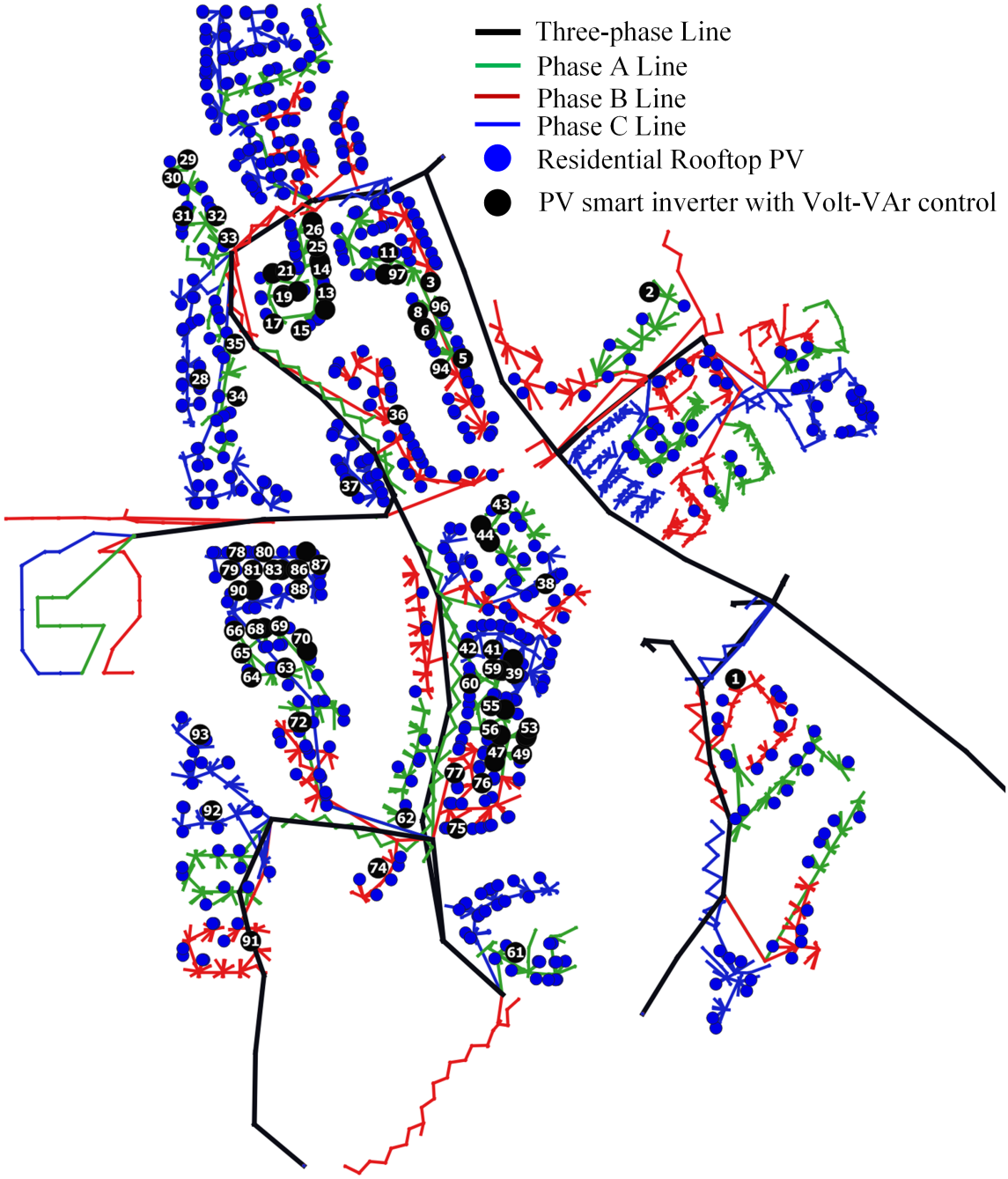

Figure 2.3: The Optimal Locations of PV Smart Inverters with Volt-VAr Control

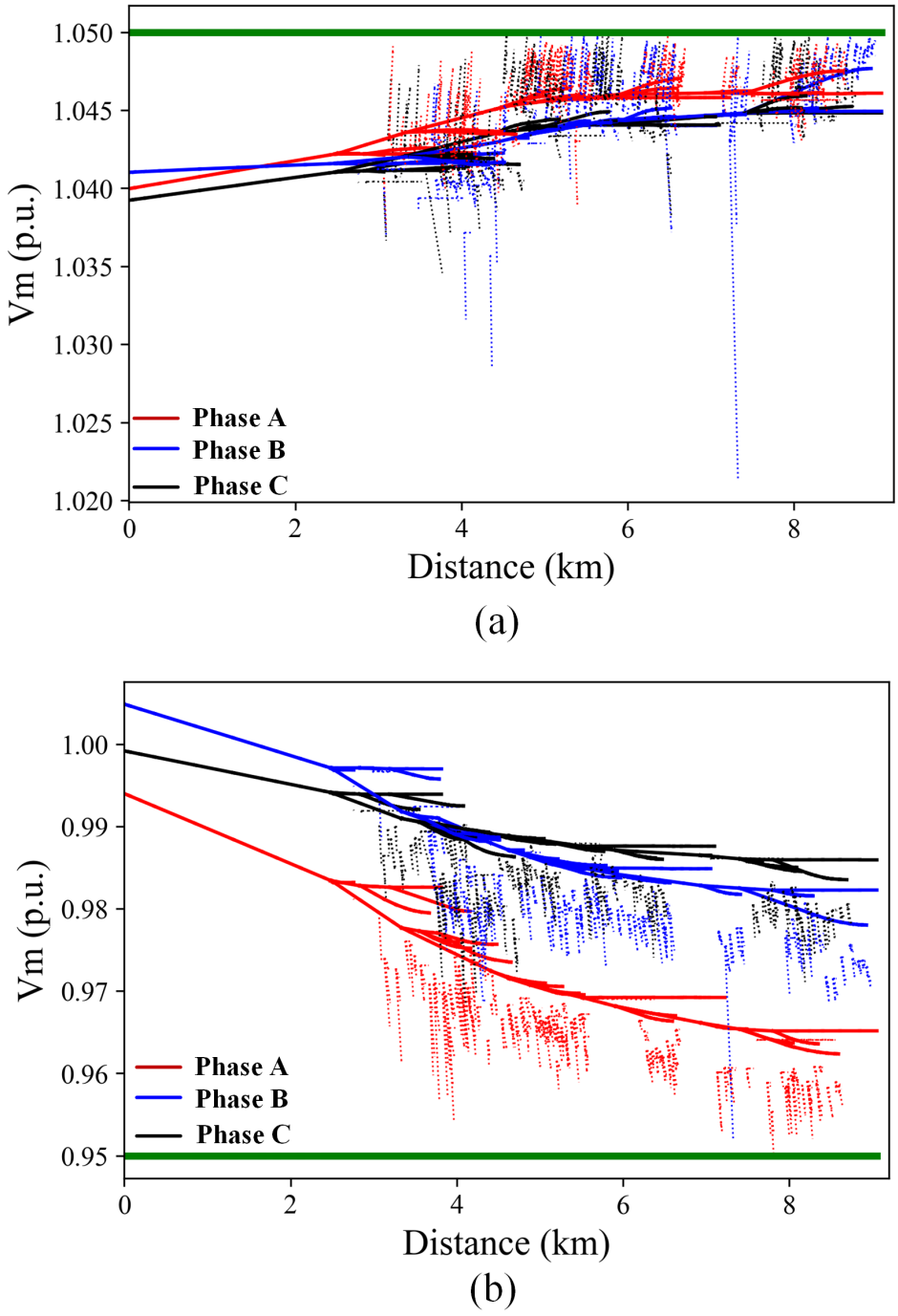

Figure 2.4: Voltage Profile After Enabling the Optimally Placed Volt-VAr Controller in (a) Over-Voltage Scenario and (b) Under-Voltage Scenario

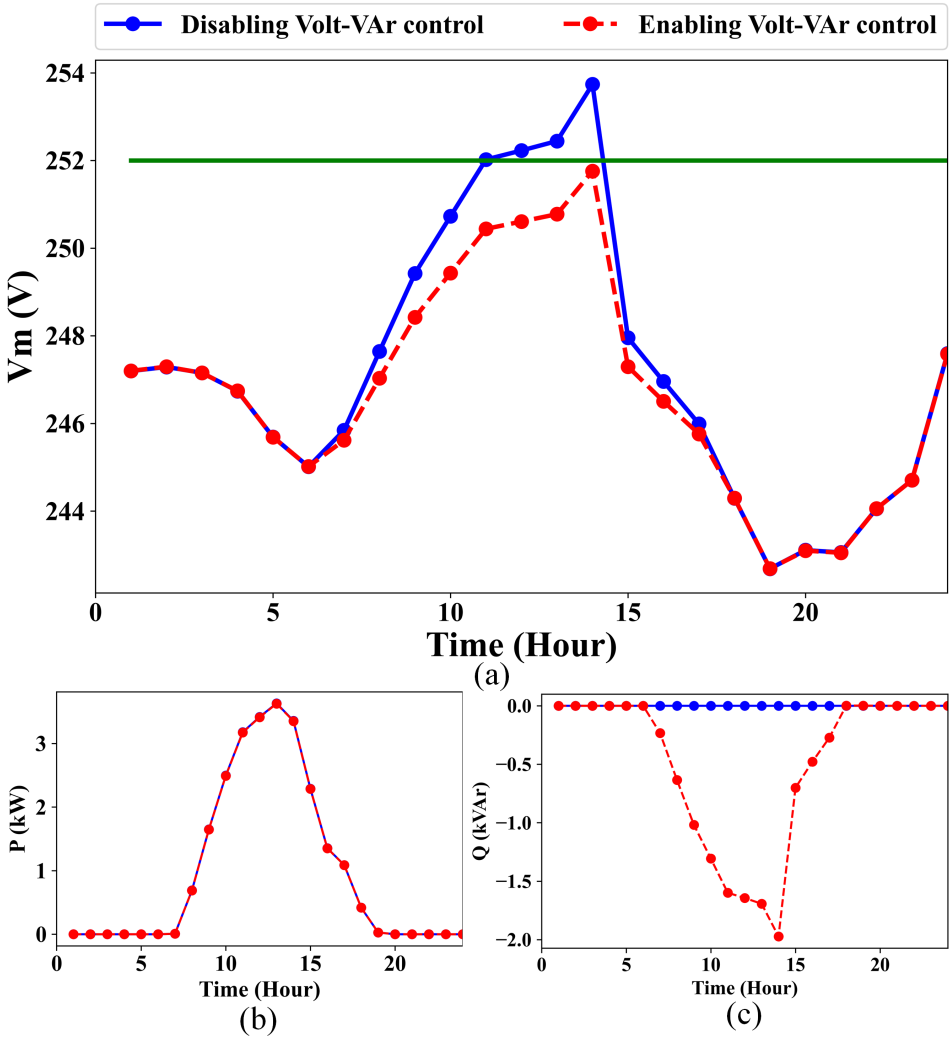

Figure 2.5: 24-hour Time-Series Voltage Magnitude, Active Power and Reactive Power Output Comparison for the 45th PV Smart Inverter Disabling and Enabling Volt-VAr Control

As only the worst voltage violation scenarios are considered, it is necessary to validate whether the optimal placement decisions work for other time instants. Two 24-hour time-series power flow studies disabling and enabling Volt-VAr control at the selected 99 PV smart inverters are conducted in the OpenDSS. Fig. 2.5 shows the hourly time-series voltage magnitude, active power output, and reactive power output comparison for the bus node with the 44th placed PV smart inverter. This specific PV bus has the maximum voltage violation in the over-voltage scenario. It is found that this bus node, when Volt-VAr control is disabled, violates the normal operation voltage limit from $t = 11$h and reaches its maximum voltage magnitude at $t = 14$h, which causes the worst over-voltage problem. With Volt-VAr enabled, there is no voltage violation issue during the entire 24-hour operation as the reactive power absorption of the PV smart inverters helps to reduce the voltage.

2.4.2 Power flow comparison between SMIP and OpenDSS

To validate the accuracy of the SMIP model, the power flow solution from the SMIP model is compared with OpenDSS after enabling Volt-VAr control in the selected PV smart inverters. Figures 2.6 (a) and (b) present the PV smart inverters' reactive power comparison between the SMIP model and OpenDSS under both scenarios. The average squared difference of the PV smart inverter's reactive power output between the SMIP model and OpenDSS is 0.548% and 0.089% respectively for the over- and under-voltage scenarios, which are relatively small values. The difference between the active power output of the smart inverters in the SMIP model and the OpenDSS in both scenarios is zero. It indicates that the optimally placed PV smart inverter with Volt-VAr control can guarantee the customers' economic benefit of maximizing their PV units' active power output even under the worst voltage scenarios. At the same time, the voltage magnitude of each bus node in both the

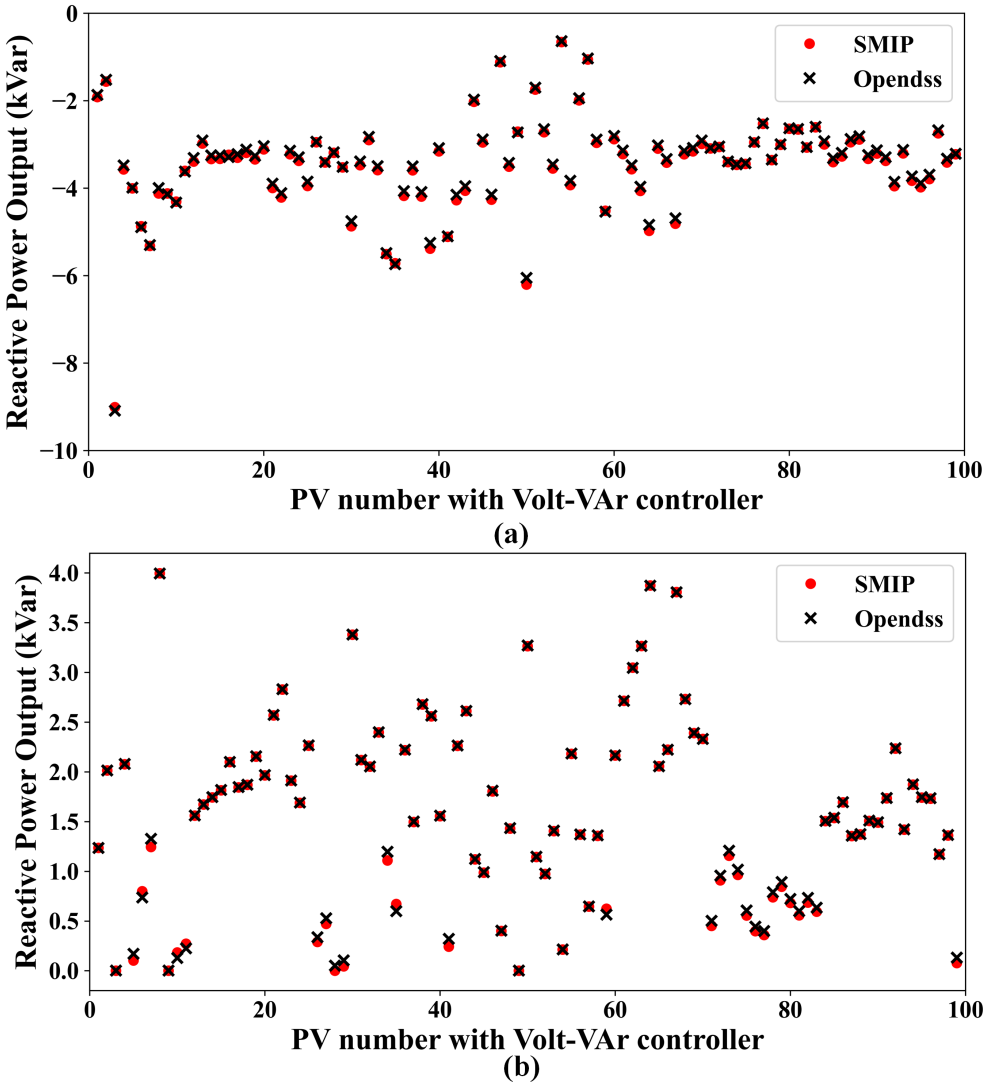

Figure 2.6: Reactive Power Output Comparison for (a) Over-Voltage Scenario and (b) Under-Voltage Scenario

SMIP model and OpenDSS are compared in Fig. 2.7. As shown in Fig. 2.7, the maximum voltage magnitude difference between the power flow solution given by the optimization program and OpenDSS is less than 1%, while the error is less than 0.1% for 99.9% of the nodes. These results validate the accuracy of the developed SMIP model in modeling the unbalanced distribution system operation considering the impact of PV smart inverter with Volt-VAr control on the system voltage profile.

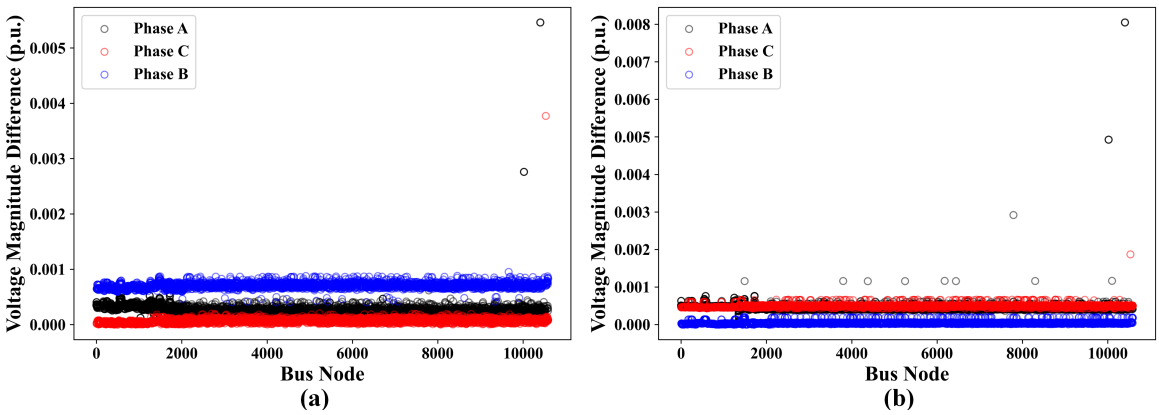

Figure 2.7: The Difference in Voltage Magnitudes Obtained From SMIP Model and OpenDSS at Each Bus for (a) Over-Voltage Scenario and (b) Under-Voltage Scenario

2.4.3 Dynamic voltage stability verification

To validate the voltage stability of the Volt-VAr control operation, a detailed dynamic model of the PV smart inverter with Volt-VAr control capability is developed based on previous work [51] in Chapter 3.

In the dynamic simulation, the optimally placed PV smart inverters are represented by the DLL developed in Chapter 3, all other PV inverters in the system are represented by the default power flow model embedded in OpenDSS. disable the Volt-VAr control at time $t = 0.0s$, then Volt-VAr control is enabled at $t = t_1$ under both scenarios. Fig. 2.8 shows the dynamic results of the 44th PV smart inverter in the over-voltage scenario, which has one of the largest voltage violations before enabling Volt-VAr control. It can be observed that a significant voltage drop is induced by the reactive power absorption of the PV smart inverter at time $t = t_1$. After the transient period, the active power can be maintained at its original value. The reactive power is kept at a higher value corresponding to the Q-V curve settings to maintain the voltage at a lower value. At $t = t_2$, the active power generations of all the 766 PVs in the system are reduced to 65% of their original output, which simulates a sudden cloud cover over the area. At $t = t_3$, the original outputs are recovered for all the PV

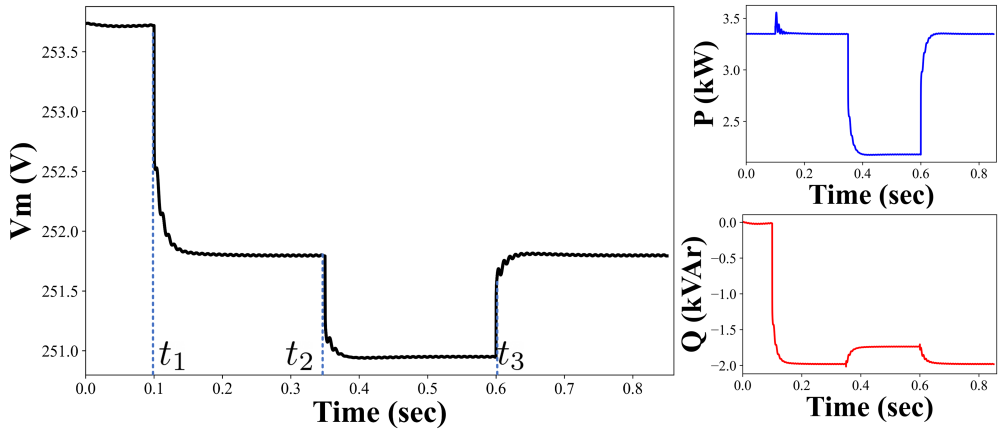

Figure 2.8: Voltage, Active and Reactive Power at the Bus Node with the 44th PV Smart Inverter in the Over-Voltage Scenario

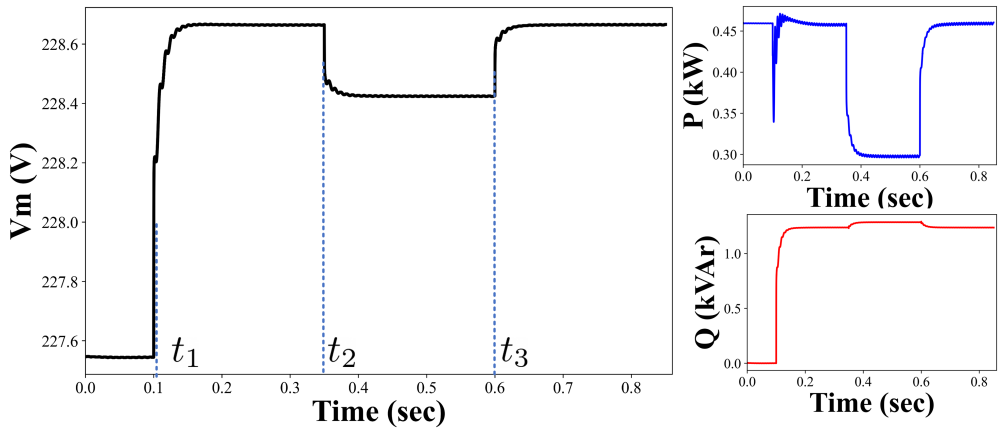

Figure 2.9: Voltage, Active and Reactive Power at the Bus Node with the 1st PV Smart Inverter in the Under-Voltage Scenario

systems. In this over-voltage scenario, active power reduction helps further reduce the voltages along the feeder, and as a result, the reactive power absorption reduces following the voltage reduction.

Similarly, Fig. 2.9 shows the dynamic results of the 1st PV smart inverter in the under-voltage scenario. In the under-voltage scenario, however, the active power reduction tends to make the voltage even lower. The presence of the volt-VAr control helps maintain the voltage at a higher level by further injecting reactive power into the grid. These results show that even in a feeder such as the utility partner's feeder

used in this study with PV penetration exceeding 100%, it is possible to manage the feeder voltage profile and keep the system stable using only a relatively small number (99 of 767) of optimally placed PV smart inverters to provide Volt-VAr support.

2.5 Conclusion

A two-stage stochastic mixed-integer linear programming model is developed to determine optimal numbers and locations of PV smart inverters with Volt-VAr control to mitigate under/over voltage conditions while minimizing the active power curtailment of PV units in active unbalanced distribution networks. In the first stage, the upgrading cost of PV smart inverter with Volt-VAr control is minimized, while the second stage minimizes the expected cost of active power curtailment of PV units and considers the detailed model of Q-V curve characteristics of PV smart inverter according to IEEE 1547 standard. With the optimally upgraded PV smart inverters, the system voltage profile can be maintained within the allowable range using only the local control capability of the PV systems without any other centralized communication mechanism. Additionally, the distribution system's steady-state performance and dynamic stability with the obtained optimal locations of the PV smart inverters are evaluated by a detailed model of PV smart inverter developed in Chapter 3 under different voltage, load, and PV output scenarios. The results illustrate that the optimal location of PV smart inverters with Volt-VAr control can mitigate the worst over and under-voltage conditions of the utility feeder network within the allowable voltage requirement of the system without any PV active power curtailment. The dynamic simulation results illustrate that the system remains stable while the reactive power output of PV units is adjusted to maintain the system voltage at the normal operation range.

Chapter 3

DYNAMIC SIMULATION OF INVERTER-BASED PV SYSTEM IN DISTRIBUTION NETWORK

In this chapter, the dynamic model of the PV inverter and the dynamic simulation of the distribution system with the PV dynamic model are discussed. These elements are then used to verify the dynamic stability where the selective Volt-VAr control is applied in the distribution system as mentioned in Chapter 2.

3.1 Introduction to Dynamic Simulation in OpenDSS

There are several distribution system simulation tools such as OpenDSS [52], GridLAB-D [53], and CYMDIST [54] that have been used in various studies. In this work, OpenDSS is used to perform the dynamic study. OpenDSS is an open-source software with various simulation capabilities such as steady-sate and quasi-static time-series (QSTS) power flow analysis. A QSTS model for the inverter-based PV is available in OpenDSS for power flow analysis. Users can either use a general generator object to represent the PV active power generation with a time-series profile or use a detailed PVSystem model to capture the PV panel characteristics related to irradiance and temperature profile [55]. Dynamic simulation involving a basic electromechanical transient can also be performed in OpenDSS, but there is only one simple built-in generator model with basic machine dynamics [56]. As OpenDSS does not provide an embedded dynamic inverter-based PV model, users need to develop their own DLL with any sophisticated model as needed.

The interaction between the OpenDSS main engine and the user-defined DLL can be described as depicted in figure 3.1. There are three main user-defined functions

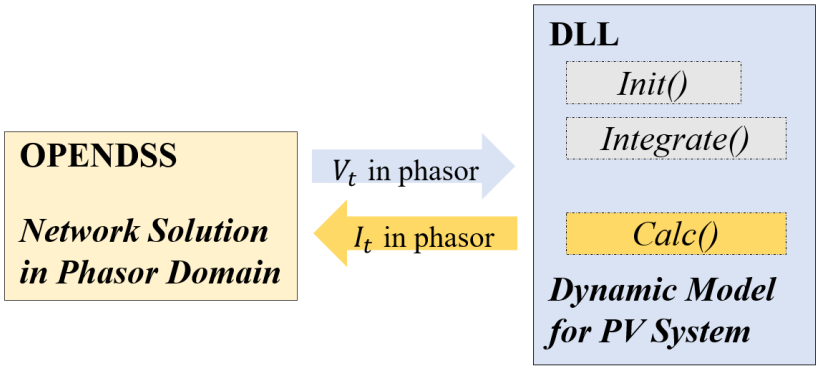

Figure 3.1: Interaction Between OpenDSS Main Engine and the User-Defined DLL

within the DLL related to the dynamic state variable calculation: (1) *Init*(), (2) *Integrate*(), and (3) *Calc*(). The *Init*() function initializes all the state variables as well as the algebraic variables in the dynamic model. The *Integrate*() function performs the actual state variable integration using the derivatives calculated from the model differential equations [57]. Users should formulate the differential equations derived from the actual PV system model into this function. The *Calc*() function updates the terminal voltage in the DLL and calculates the terminal current from the integration results then returns the current to the OpenDSS main engine. Other functions like creating and erasing the model instance and reading and writing the data should also be represented in the DLL, which are not explicitly illustrated here.

3.2 Time-Domain Inverter-Based PV Model

Fig. 3.2 shows the simplified block diagram of the inverter power stage used for verification in Chapter 2, which can be numerically implemented in the DLL using differential equations represented by system state variables and parameters. The PV inverter contains 5 blocks: (1) pulse-width modulation (PWM) converter, (2) LCL filter, (3) phase-locked loop (PLL), (4) Volt-VAr control, and (5) current control. The PWM block converter and Volt-VAr control block can be represented by several algebraic functions, while the LCL, PLL, and current control blocks introduce state

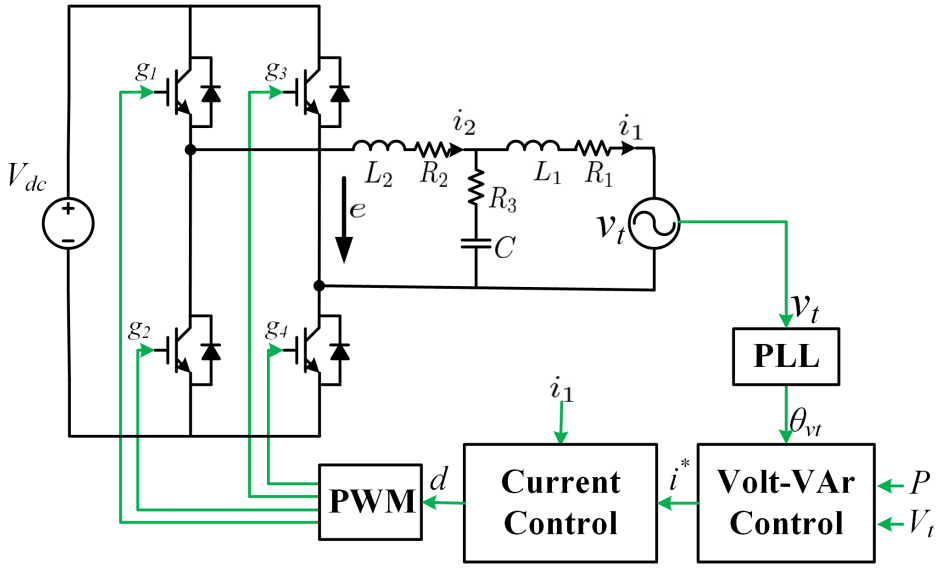

Figure 3.2: Block Diagram of the PV Inverter

variables to the dynamic system and can be represented by a set of differential equations. The LCL filter is a linear system that can be represented by linear differential equations. There are various kinds of current control including linear control functions or even nonlinear control functions, which will be introduced in the following sections.

3.2.1 PV inverter with linear control functions

The LCL filter circuit in Fig. 3.2 contains 3 state variables: i_1, i_2 and v_C. From Kirchhoff's voltage law, the LCL filter block can be written as a set of differential equations:

$$\dot{i_1} = -\frac{R_C + R_1}{L_1} i_1 + \frac{R_C}{L_1} i_2 + \frac{1}{L_1} v_C - \frac{1}{L_1} v_t \tag{3.1}$$

$$\dot{i_2} = -\frac{R_C + R_2}{L_2} i_2 + \frac{R_C}{L_2} i_1 - \frac{1}{L_2} v_C + \frac{1}{L_2} e \tag{3.2}$$

$$\dot{v_C} = \frac{1}{C} i_2 - \frac{1}{C} i_1 \tag{3.3}$$

The PLL block which is shown in detail in Fig. 3.3 is used to extract the reference

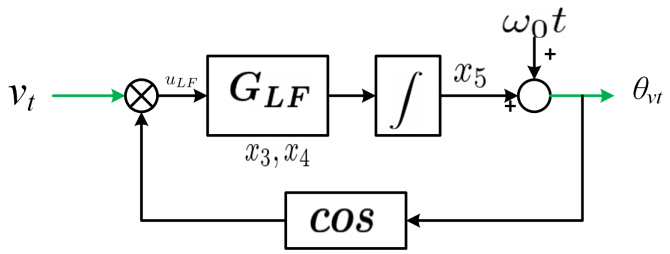

Figure 3.3: Block Diagram of the PLL

angle θ_{vt} from the terminal voltage v_t. The transfer function for the second order loop filter is G_{LF}:

$$G_{LF} = 4.7\frac{s + 3.37}{s^2 + 46.9s} \tag{3.4}$$

The order of the entire PLL block is 3, let x_3, x_4 and x_5 be the state variables for this control block, then the differential equations for the PLL can be written as:

$$\dot{x_3} = -46.9x_3 + 2u_{LF} \tag{3.5}$$

$$\dot{x_4} = x_3 \tag{3.6}$$

$$\dot{x_5} = 2.357x_3 + 7.938x_4 \tag{3.7}$$

the extracted voltage angle can be written as:

$$\dot{\theta_{vt}} = 2.357x_3 + 7.938x_4 + 2\pi 60 \tag{3.8}$$

The detailed Volt-VAr control block is shown in Fig. 3.4. This block does not contain any integration procedure, only algebraic calculation is involved, it does not add extra state variables to the inverter model. The inverter's active and reactive power output can be controlled to conduct various grid support functions by adjusting the active current and the reactive current separately. The Volt-VAr control block controls the power output by automatically adjusting the current reference i^* according to the terminal voltage $V_t \angle \theta_{vt}$. The scheme shown in Fig. 3.4 corresponds to reactive power priority mode, and hence, the active power output may be curtailed if the inverter does not have enough capacity.

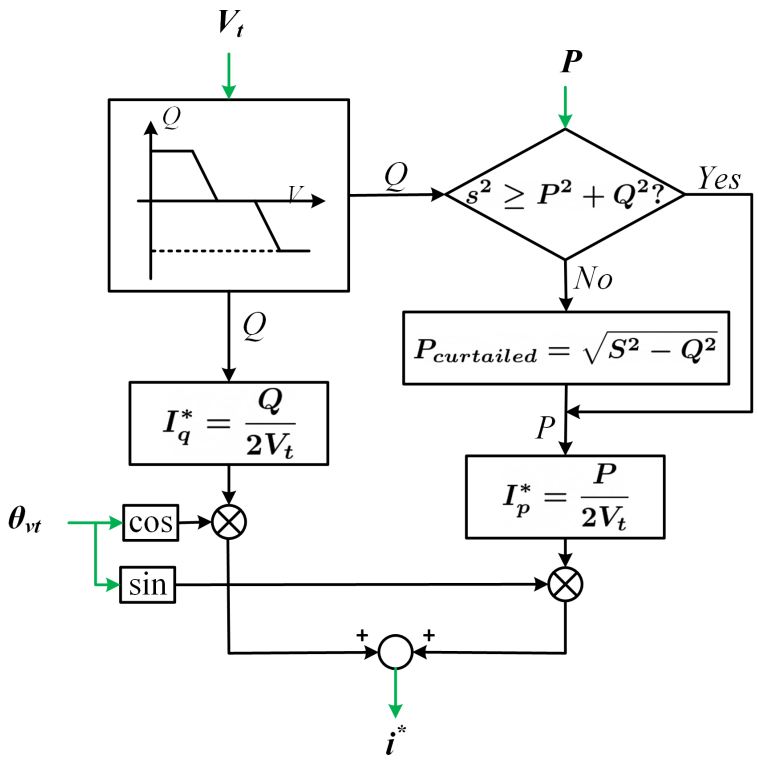

Figure 3.4: Block Diagram of the Volt-VAr Control Block

The Proportional-Resonant (PR) current control is a typical linear current control function that can force the grid-side inductor current, that is, the terminal current i_t of the inverter, to follow the current reference i^* provided by the Volt-VAr control block. The block diagram for PR current control is shown in Fig. 3.5, in which $K_p = 0.7$ is the proportional gain, and $K_r = 200$ is the resonant gain. $\omega_0 = 2\pi 60$ is the resonant frequency. V_{dc} is the DC link voltage and d is the duty cycle fed into the PWM block. The order for the PR current control block is 2, let x_1 and x_2 be the state variables for this block, then the differential equations for x_1 and x_2 can be written as:

$$\dot{x_1} = -0.6x_1 - 277.6x_2 + i^* - i_1 \tag{3.9}$$

$$\dot{x_2} = 512x_1 \tag{3.10}$$

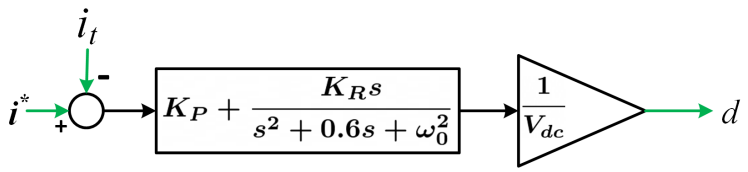

Figure 3.5: Block Diagram of the PR Current Control

The duty ratio d and the voltage e interfaced to the grid-connected LCL filter can be written as follows by using the average model of the PWM converter.

$$d = \frac{1}{V_{dc}}(K_R x_1 + K_P(i^* - i_1)) \tag{3.11}$$

$$e = V_{dc} d \tag{3.12}$$

3.2.2 PV inverter with nonlinear control functions

As the PV control techniques evolve rapidly, there is a need to implement nonlinear controllers in the PV model. For example, [39] applied adaptive nonlinear control to grid-connected PV in weak distribution grids to accommodate various grid impedances. The current control scheme proposed in [39] with model reference adaptive control (MRAC) as an inner control loop is shown in figure 3.6, which can be applied to the PR current control introduced in section 3.2.1, with all the blocks in figure 3.2 remaining the same except the current control block. The detailed control scheme is shown in figure 3.7.

The reference model $W_m(s)$ can be represented by the following transfer function,

$$W_m(s) = \frac{1}{L_m s + R_m} \tag{3.13}$$

which generates the desired response i_m for the plant and introduces a new state variable i_m to the PV inverter model built in section 3.2.1:

$$\dot{i}_m = \frac{1}{L_m}(-r_m i_m + v_{ir}) \tag{3.14}$$

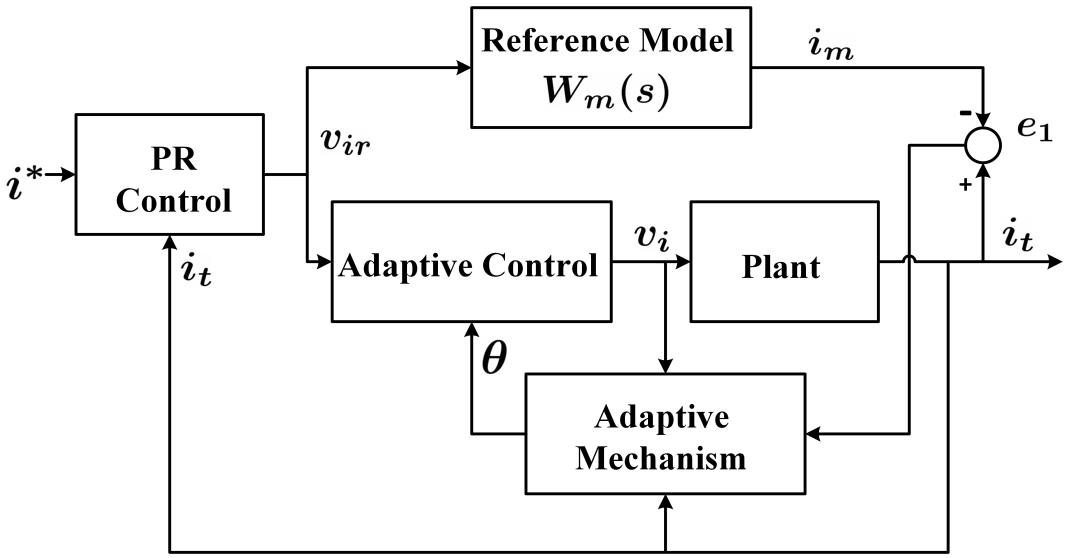

Figure 3.6: Current Control Scheme with MRAC as an Inner Control Loop

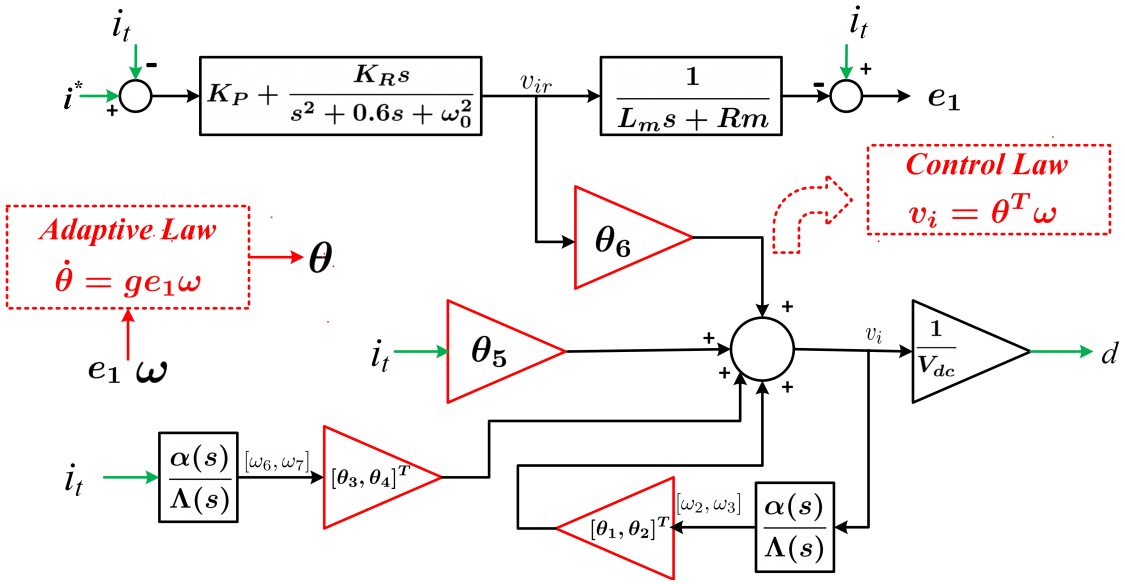

Figure 3.7: Current Control Scheme with MRAC Applied in PV Inverter

v_{ir} is the output of the PR controller and the input for the reference model $W_m(s)$.

The plant includes the LCL filter as well as the grid impedance connected to the PV inverter grid interface. The error $e_1 = i_t - i_m$ represents the difference between the actual plant output i_t, that is, the terminal current for the PV inverter, and the desired response. The error e_1 should be 0 when the system reaches its steady state. As a result, the adapted parameter vector $\boldsymbol{\theta}$ for the controller can be automatically tuned to adapt to various operational conditions with different grid impedance.

With the assumptions described in [39], the control law can be given by

$$v_i = \boldsymbol{\theta}^T \boldsymbol{\omega}. \tag{3.15}$$

$\boldsymbol{\theta} = [\theta_1, \theta_2, \theta_3, \theta_4, \theta_5, \theta_6]^T$ is the adaptive controller parameter vector and is adjusted by the following adaptive law:

$$\dot{\boldsymbol{\theta}} = g e_1 \boldsymbol{\omega} = g(i_t - i_m)\boldsymbol{\omega}, \tag{3.16}$$

in which $i_t = i_1$, i_1 is one state variable introduced in the previous section. Let $g = -20$ and obtain a decoupled adaptive law. Since θ_1 - θ_6 are variable parameters, they should be treated as new state variables to the PV inverter model. $\boldsymbol{\omega} = [\omega_2, \omega_3, \omega_6, \omega_8, i_t, v_{ir}]^T$ is the vector that contains the internal states of the adaptive mechanism, the actual response of the plant, and the input for the reference model.

$$v_{ir} = K_R x_1 + K_P(i^* - i_t), \tag{3.17}$$

which is similar to voltage e in equation (3.12).

In figure 3.7, both $\frac{\alpha(s)}{\Lambda(s)}$ blocks can be written as

$$\frac{\alpha(s)}{\Lambda(s)} = [\frac{s}{s^2 + s + 1}, \frac{1}{s^2 + s + 1}], \tag{3.18}$$

which introduces 8 state variables ω_1 - ω_8 to the model:

$$\dot{\omega}_1 = \omega_2, \tag{3.19}$$

$$\dot{\omega}_2 = v_i - \omega_2 - \omega_1, \tag{3.20}$$

$$\dot{\omega}_3 = \omega_4, \tag{3.21}$$

$$\dot{\omega}_4 = v_i - \omega_4 - \omega_3, \tag{3.22}$$

$$\dot{\omega}_5 = \omega_6, \tag{3.23}$$

$$\dot{\omega}_6 = i_t - \omega_6 - \omega_5, \tag{3.24}$$

$$\dot{\omega}_7 = \omega_8, \tag{3.25}$$

$$\dot{\omega}_6 = i_t - \omega_8 - \omega_7, \tag{3.26}$$

With the extra differential equations derived in this section for the MRAC scheme, 15 extra state variables are introduced based on the model described in section 3.2.1. The variable parameters θ_1 - θ_6 have the corresponding nonlinear differential equations (3.16) for the adaptive law. These introduce nonlinearities to the PV inverter model hence the PV system with the MRAC scheme should not be represented by phasor equations in dynamic simulations.

3.3 Dynamic Phasor Transformation of Time-Domain PV Inverter Model

Phasors are used to represent the magnitude and the angle of the fundamental frequency components of the variables in the power system simulations where fast transients can be neglected. Some dynamic models of the devices in the power system can be directly derived with phasors like the synchronous machine. But for power electronic devices like grid-connected inverters, which are usually modeled using time-domain real-valued signals, a transformation from the real-valued model is necessary to get a phasor model. With the phasor model for PV inverter, dynamic simulation can be conducted in phasor-domain simulation tools like OpenDSS to examine the impact on voltage stability by high penetration of PV resources in the distribution system.

The dynamic phasor (DP) of a signal $x(t)$ is defined as the $h-th$ complex coefficients of the Fourier series expansion over the time window $(t, t-T]$. The calculation for $h-th$ dynamic phasor is depicted in (3.27), which can also be written in the form of (3.28). R and I indicate the real and the imaginary part of the complex phasor, respectively. Time t is omitted in (3.28), and will be omitted in the development that follows.

$$\bar{x}_h(t) = \frac{1}{T}\int_0^T X(T-t+\tau)e^{-jh\omega_0(t-T+\tau)}d\tau \tag{3.27}$$

$$\bar{x}_h = x_h^R + jx_h^I \tag{3.28}$$

When the signal $x(t)$ is strictly periodic, the resulting DPs are identical to the ones obtained by the conventional Fourier series expansion. The differentiation of the dynamic phasor can be written as:

$$\frac{d\bar{x}_h}{dt} = -jh\omega_0\bar{x}_h + f(\bar{x}_h, \bar{u}_h) \tag{3.29}$$

$$f(x,u) = \frac{dx}{dt} \tag{3.30}$$

For a linear system like the PV inverter with PR current controller introduced in this section, the time-domain real-valued model can be easily transformed into a dynamic phasor model with only the fundamental frequency component. The system differential equations for the PV inverter can be rewritten as:

$$\frac{d\bar{i}_1}{dt} = -j\omega_0\bar{i}_1 - \frac{R_C+R_1}{L_1}\bar{i}_1 + \frac{R_C}{L_1}\bar{i}_2 + \frac{1}{L_1}v_C - \frac{1}{L_1}\bar{v}_t \tag{3.31}$$

$$\frac{d\bar{i}_2}{dt} = -j\omega_0\bar{i}_2 - \frac{R_C+R_2}{L_2}\bar{i}_2 + \frac{R_C}{L_2}\bar{i}_1 - \frac{1}{L_2}\bar{v}_C + \frac{1}{L_2}\bar{e} \tag{3.32}$$

$$\frac{d\bar{v}_C}{dt} = -j\omega_0\bar{v}_C + \frac{1}{C}\bar{i}_2 - \frac{1}{C}\bar{i}_1 \tag{3.33}$$

$$\frac{d\bar{x}_1}{dt} = -j\omega_0\bar{x}_1 - 0.6\bar{x}_1 - 277.6\bar{x}_2 + \bar{i}^* - \bar{i}_1 \tag{3.34}$$

$$\frac{d\bar{x}_2}{dt} = -j\omega_0\bar{x}_2 + 512\bar{x}_1 \tag{3.35}$$

$$\bar{d} = \frac{1}{V_{dc}}(K_R\bar{x}_1 + K_P(\bar{i}^* - \bar{i}_1)) \tag{3.36}$$

$$\bar{e} = V_{dc}\bar{d} = K_R\bar{x}_1 + K_P(\bar{i}^* - \bar{i}_1) \tag{3.37}$$

All the state variables are represented by complex phasors in equation (3.31)-(3.37). The complex phasor equation should be decomposed into its real and imaginary parts separately when implemented in the DLL integrate function. The equations for the PLL block remain in the time domain to track the instantaneous angle of the PV inverter terminal voltage and feed that angle information into the phasor domain equations.

For a nonlinear system like the PV inverter with the MRAC scheme introduced in this section, harmonic signals with various frequency components other than the fundamental frequency could be generated. In the MRAC scheme, the nonlinearities are generated by the product of two state variables in equation 3.16. In the phasor domain, the h^{th} order product of two dynamic phasors $\bar{x}$ and $\bar{y}$ can be calculated as

$$(\bar{x} \cdot \bar{y})_h = \sum_{i=-\infty}^{+\infty} \bar{x}_{h-i}\bar{y}_i. \tag{3.38}$$

The right term of (3.38) contains a broad spectrum of the signal generated by the product of two signals. It is necessary to capture all the frequency components that dominate the performance in the right term of (3.38) when the nonlinear system is modeled in the phasor domain. However, the number of system equations will be multiplied by the number of the different frequencies considered, which is complicated and will introduce a large computational burden.

3.4 Hybrid Simulation of Time-domain PV Inverter Model and Phasor-Domain Network in OpenDSS

PV inverter models with linear control functions can be easily transformed from the time-domain model to the phasor-domain model using dynamic phasor transformation because linear models can be represented using single-frequency phasors. However, harmonic signals with various frequencies could be generated in nonlinear models, and as a result, single-frequency phasors are not sufficient to represent the nonlinear model dynamics. It is necessary to represent all the frequency components that dominate the model dynamics in phasor-domain models, however, it is difficult to capture a broad spectrum of the model transients with a limited amount of frequency components considered. In such cases, the simulation of transient waveforms (i.e., time-domain EMT model) is required to capture all the necessary dynamics[7]. To accommodate the time-domain model in OpenDSS simulation, a hybrid model should be developed in the DLL that can both do the time-domain simulation and exchange data between the time-domain model and the phasor-domain network in OpenDSS using a proper phasor extraction technique.

3.4.1 Phasor extraction based on SOGI-PLL

In order to achieve a hybrid simulation with the time-domain model in DLL and the phasor network in OpenDSS, a second-order generalized integrator (SOGI) based PLL is used to extract the magnitude and the phase angle of the instantaneous current signal in the time-domain model. In the aspect of dynamic modeling in DLL, two extra algorithms are added to the original DLL functions $Integrate()$ and $Calc()$ as shown in figure 3.8.

The schematic for the SOGI-PLL is shown in figure 3.9. There are 4 new state

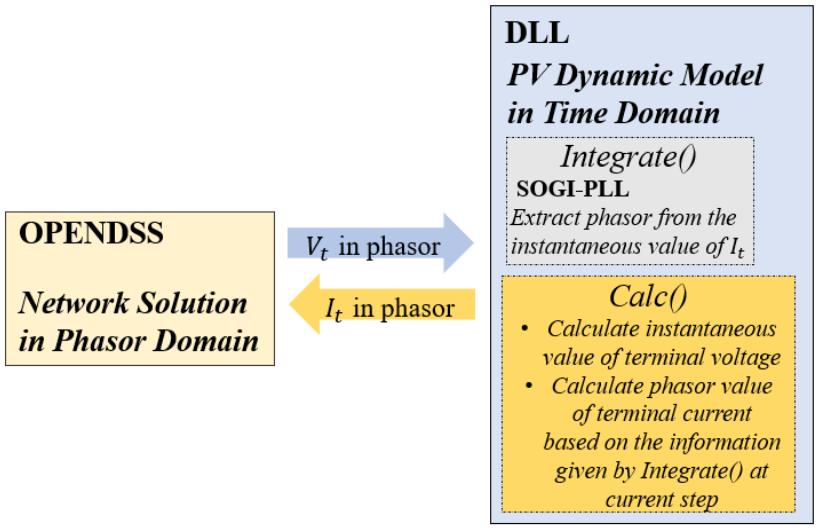

Figure 3.8: Interaction Between OpenDSS Main Engine and the User-Defined DLL

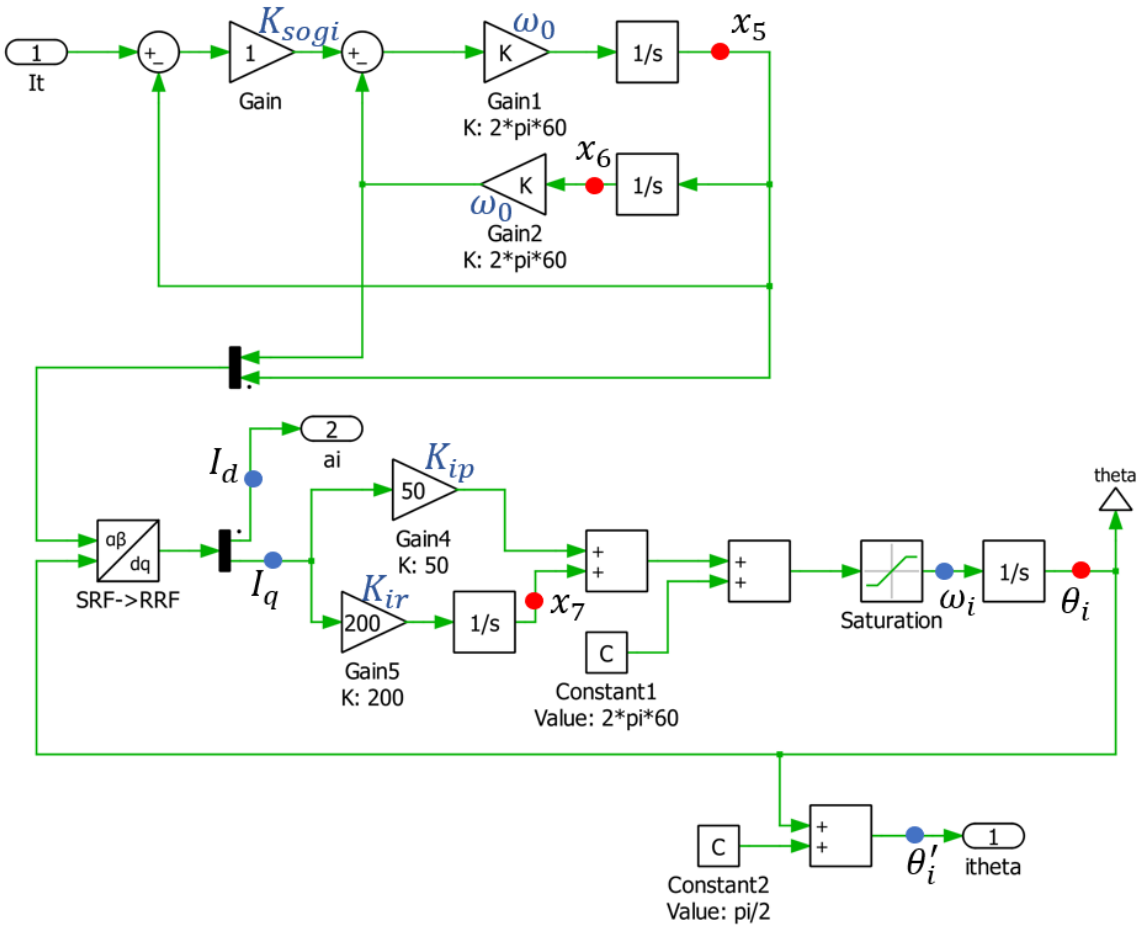

Figure 3.9: Current Phasor Extraction Based on SOGI-PLL

variables introduced by the SOGI-PLL which are marked by the red dots in figure 3.9. The differential equations can be derived as follows:

$$\frac{dx_5}{dt} = K_{sogi}\omega_0(I_1 - x_5) - \omega_0^2 x_6, \tag{3.39}$$

$$\frac{dx_6}{dt} = x_5, \tag{3.40}$$

$$\frac{dx_7}{dt} = K_{ir} I_q, \tag{3.41}$$

$$\frac{d\theta_i}{dt} = \omega_i. \tag{3.42}$$

The algebraic variables are marked by the blue dots in figure 3.9 and the equations can be written as follows:

$$I_d = x_5 cos\theta_i + \omega_0 x_6 sin\theta_i, \tag{3.43}$$

$$I_q = \omega_0 x_6 cos\theta_i - x_5 sin\theta_i, \tag{3.44}$$

$$\omega_i = 2\pi 60 + x_7 + K_{ip} I_q, \tag{3.45}$$

$\omega_0 = 2\pi 60$. θ_i in the above equations has a 90° deviation with the actual current phase angle $\theta_i^{'} = \theta_i + \frac{\pi}{2}$. The extracted current magnitude a_i is equal to I_d.

The equations for the SOGI-PLL are implemented in the $Integrate()$ function in the DLL, which are treated in the same manner as the equations for the PV inverter. The current phase angle is treated as a new state variable while the current magnitude can be calculated using the new state variables introduced by the SOGI-PLL. The data exchange function between the phasor domain and the time domain is implemented in the $Calc()$ function as shown in figure 3.8.

3.4.2 Simulation results

A small system with 7 PV inverters and one distribution transformer is built for the hybrid simulation verification of the time-domain model in OpenDSS. PLECS is a

simulation tool designed for power electronic simulation, which is used in this section for the verification of the developed OpenDSS dynamic models.

PV inverter with PR current control

The same simulations are conducted on the 7-PV small system with the PV model represented in the time domain and phasor domain in OpenDSS. The whole 7-PV system is also built in PLECS to verify the simulation results in OpenDSS. Figure 3.10 shows the results for one PV inverter in the small system from different cases in one plot. At $t = 0.25s$, the source voltage to which the distribution transformer is connected is increased from $1p.u.$ to $1.1p.u.$; at $t = 0.5s$, the Volt-VAr control is enabled for all the PV inverters. Reactive power generation is set as a priority in the Volt-VAr control, so after $t = 0.5s$, the active power is curtailed to 0. As the result shows, the simulation of the time-domain model matches with the Phasor-domain model and the simulation in PLECS when the system reaches its steady state. The minor differences in transients can be ignored. The differences can result from the different representations of the signals in different simulation setups. The black solid line represents the PV time-domain model, the simulation is a hybrid simulation between the time-domain PV model and the phasor domain network in OpenDSS. The green line represents the PV phasor-domain model, the simulation is purely in the phasor domain, while the red dotted line represents the PLECS simulation which is entirely in the time domain.

Simulations for the time-domain and phasor-domain model in OpenDSS are also conducted on the over-voltage scenario of the large-scale actual utility system introduced in section 2.3. The comparison of the results is shown in figure 3.11. At $t = 0.3s$, the Volt-VAr control is enabled for all the smart inverters; at $t = 0.6s$, the active power generation of all the PVs in the system is reduced to 65% to simulate

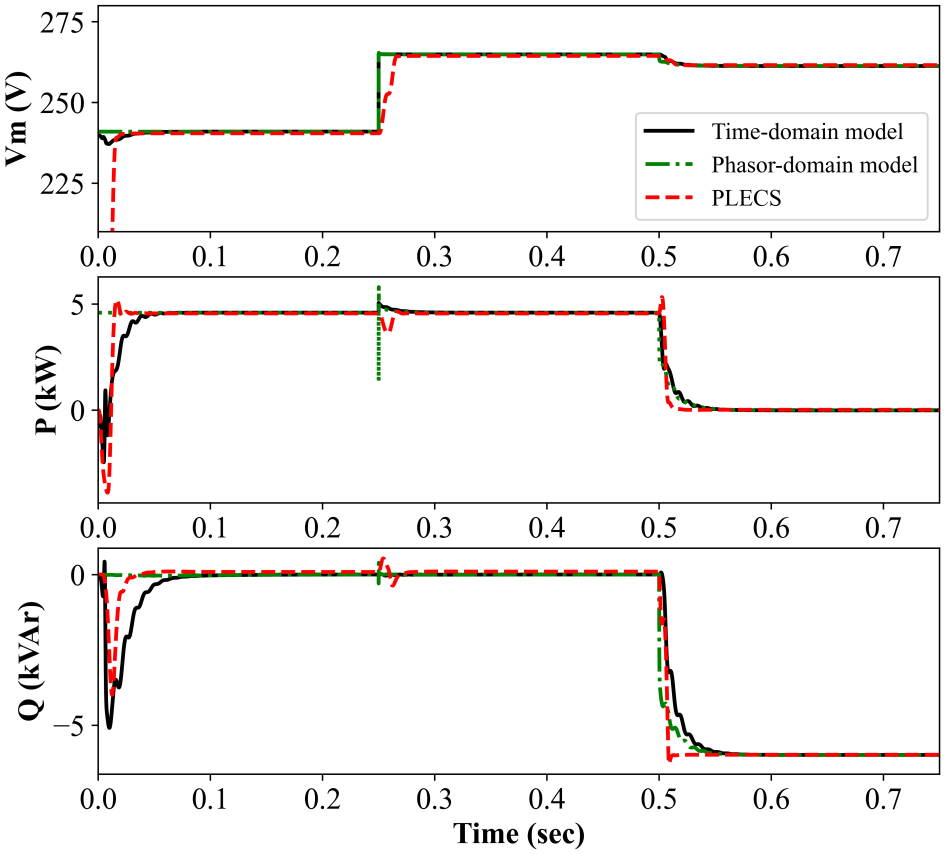

Figure 3.10: Simulation Results Comparison for the PV Inverter with PR Current Control

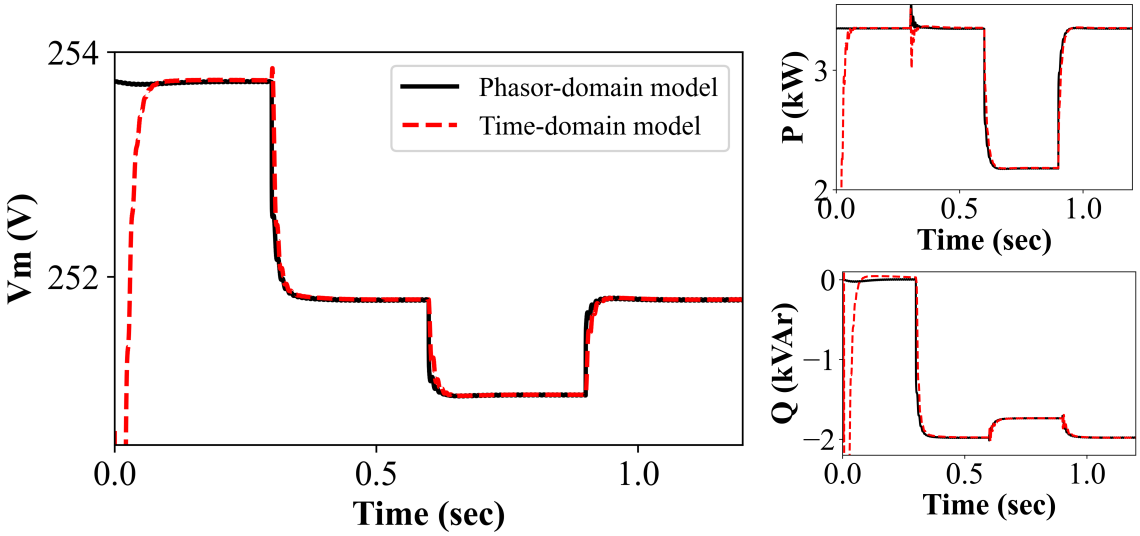

Figure 3.11: Large System Simulation Results Comparison for the PV Inverter with PR Current Control

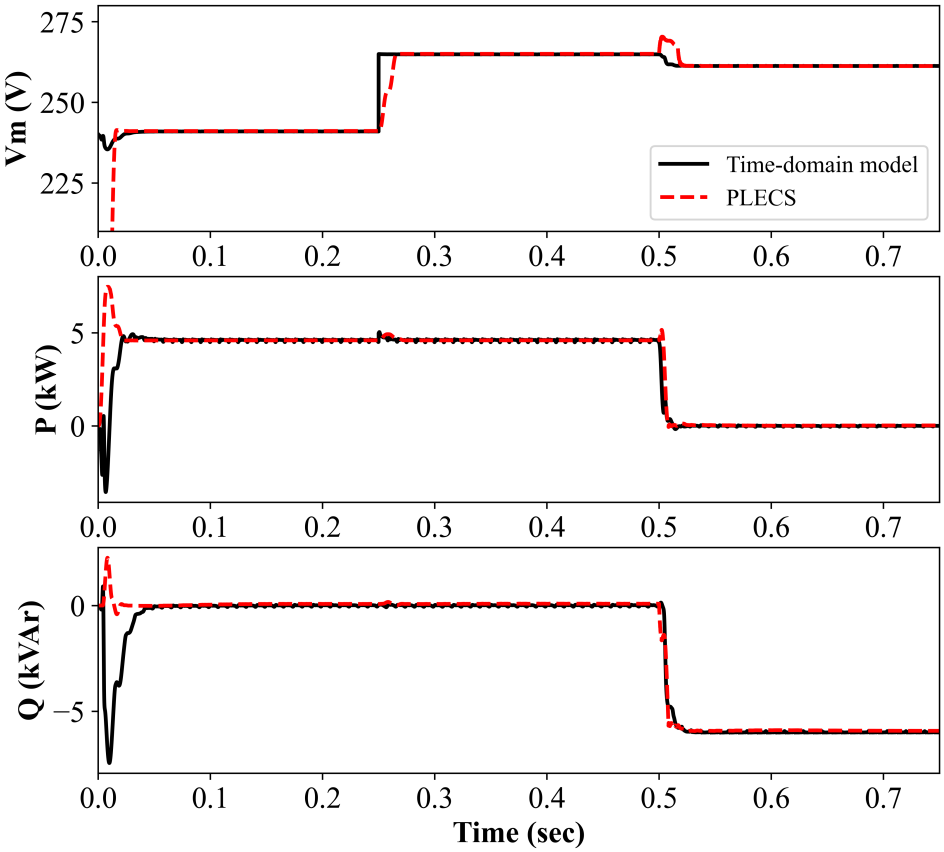

Figure 3.12: Simulation Results Comparison for the PV Inverter with MRAC Current Control

a sudden cloud cover of the entire area; at $t = 0.9s$, the active power generation is recovered. The results show that the time-domain model also matches with the phasor-domain model in large-scale system simulations.

PV inverter with MRAC current control

The same simulations are conducted on the 7-PV small system with the PV model represented in the time domain in OpenDSS and in PLECS. The results are shown in figure 3.12. The simulation results of the time-domain model in OpenDSS match with the result in PLECS simulation, which illustrates that the nonlinear functions could be implemented accurately by the time-domain model in the DLL and dynamic

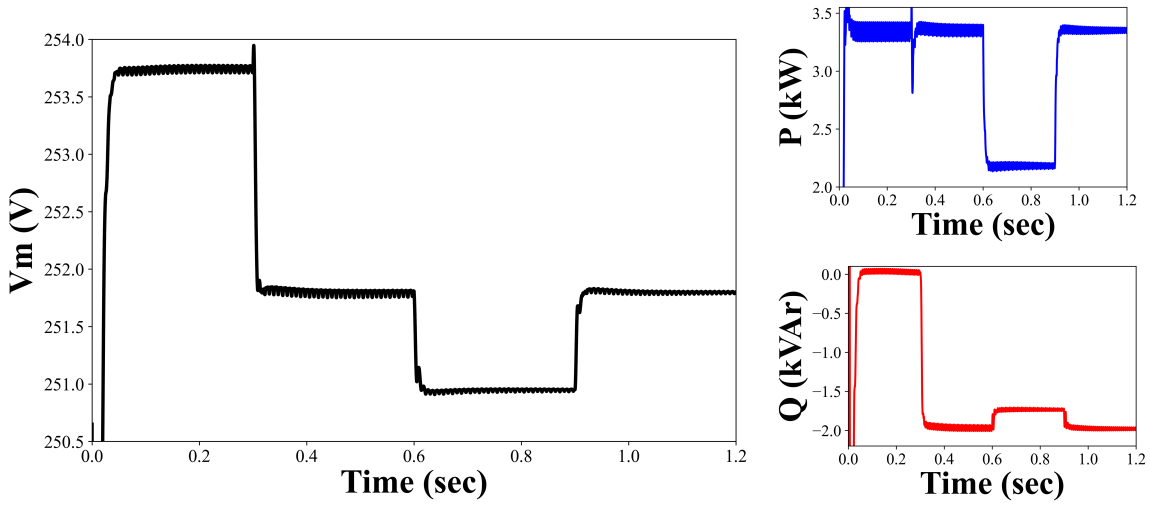

Figure 3.13: Large System Simulation Results for the PV Inverter with MRAC Current Control

stability of the nonlinear model can be verified using a time-phasor-domain hybrid simulation.

Simulations for the nonlinear time-domain model in OpenDSS are also conducted on the over-voltage scenario of the large-scale actual utility system. The results are shown in figure 3.13. There are minor oscillations in the power output of the PV inverter, but the decay of the oscillations can be observed with time.

3.5 Conclusion

In this chapter, detailed dynamic models of the PV smart inverter with Volt-VAr control capability are developed to test the dynamic impact of the PV smart inverters on the distribution system in OpenDSS. PV inverter models with linear control functions can be easily represented by a phasor-domain model, while nonlinear control functions should be represented in the time domain to capture all the necessary transients in dynamic studies. Since OpenDSS is a phasor-based simulation tool, a time-domain model with a phasor extraction function is developed in this chapter for the PV inverters with nonlinear control functions. Hybrid simulation can be achieved

with the OpenDSS main engine and the user-define DLL for the PV inverter model represented in the time domain. The developed time-domain dynamic model for the PV inverter is tested in OpenDSS dynamic simulation, and the simulation results are compared with the phasor-domain model and PLECS simulation. For the time-domain model with linear control function, the results are matched with both the phasor-domain model simulation in OpenDSS and the PLECS simulation. For the time-domain model with nonlinear control functions, the results are matched with the PLECS simulation. The results verify the effectiveness of the developed time-domain model.

Chapter 4

INTEGRATIVE DYNAMIC SIMULATION FRAMEWORK IN OPENDSS

4.1 Overview of the Dynamic Simulation Framework in OpenDSS

The basic algorithm for dynamic integration in OpenDSS is a fixed-step size predictor-corrector method with one step of correction. There are three main functions within the DLL related to the dynamic state variable calculation as described in section 3: (1) $Init()$ (2) $Integrate()$ (3) $Calc()$. Both the predictor and the corrector formula should be defined in function $Integrate()$ by the users.

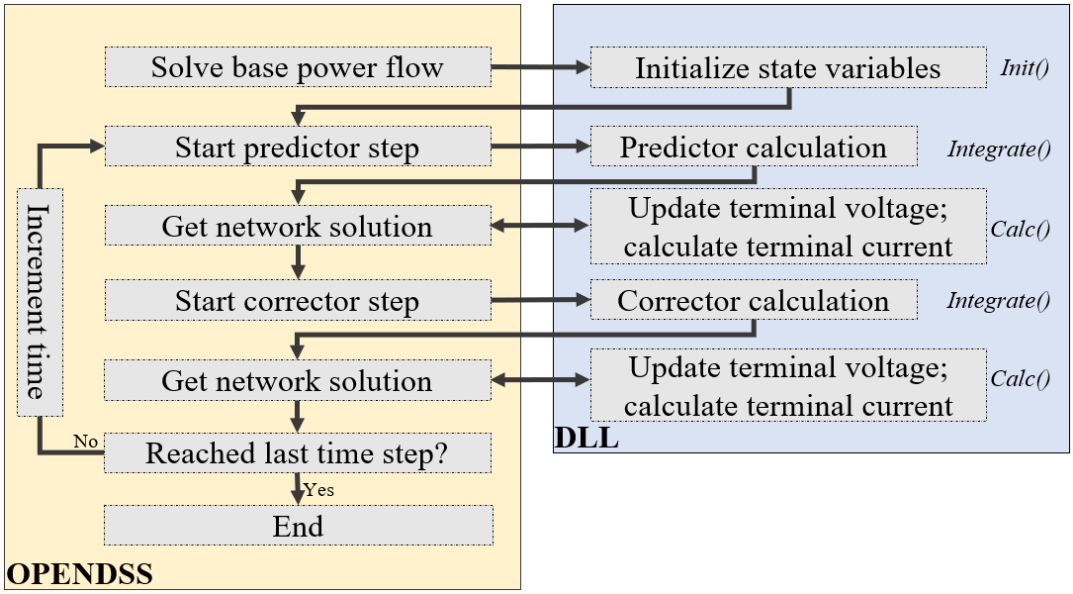

Figure 4.1: Original Framework of OpenDSS and DLL in Dynamic Mode

Fig. 4.1 shows the simplified interaction framework of OpenDSS and the user-defined DLL in dynamic mode, taking only the iteration process into account. OpenDSS is the host application that actually calls the user-defined functions implemented in the DLL. When multiple PV models exist in the distribution feeder, the OpenDSS

main engine can create multiple PV model instances based on just one DLL as long as all the PVs have the same model structure and parameters. All the PV model instances as well as the distribution feeder model in OpenDSS form the network solution. The dynamic simulation step size and the total number of steps can be determined by the users in the OpenDSS main program. The simulation time increments at each iteration until the step counts reach the total number of steps. All the PV models and the feeder model are simulated using the same fixed-step size, which is always set close to the maximum step size allowed to keep the simulation numerically stable. Using a user-defined model is straightforward to simulate the dynamic impact of inverter-based PVs in large-scale distribution systems using OpenDSS, but the model transient complexity constrains the maximum allowed simulation step size. Since OpenDSS only has a fixed-step size dynamic simulation framework, the whole system needs to be simulated using a fixed-time step which has to be small enough to keep the simulation numerically stable. This step size could be unnecessarily small when the system reaches a steady state.

4.2 Adaptive Step Size Simulation Framework

An adaptive step size simulation framework is developed in OpenDSS in this report, which automatically adjusts the step size during the simulation by evaluating the dynamic differential equations for each PV instance at each time interval. As a result, the simulation only uses the small step size when it is necessary, otherwise, a larger step size is used to speed up the simulation.

The Gear-Nordsieck method has proven to be a robust numerical method to solve the initial value problem in literature [58; 59]. The integrative framework utilizes the fourth-degree Gear-Nordsieck method, which is available in [60] to build the integration function in the developed DLL to achieve overall automatic step size adjustment

in OpenDSS. The detailed simulation framework is shown in Fig. 4.2. All the state variables y_i and any other integration-related variables (step size h_{pv} and Nordsieck vector $\mathbf{z}_i$) for each PV instance should be initialized before the dynamic simulation starts. At each time step, all the PV instances in the system will make an approximation of the state variables for the next time step based on the values of the current state variables and other integration variables. Gear's step size control method is applied to evaluate the Nordsieck vector for each PV instance to determine their proper step sizes h_{pv} for the current step. Those step sizes are then returned to the OpenDSS main engine. OpenDSS will adjust the overall system step size to meet the minimum requirement $h_{min,sys}$ among all the PV instance step sizes and return it back to each PV instance. Each PV instance utilizes this uniform system step size to perform the final integration and increase the step size for the next step based on the current step evaluation.

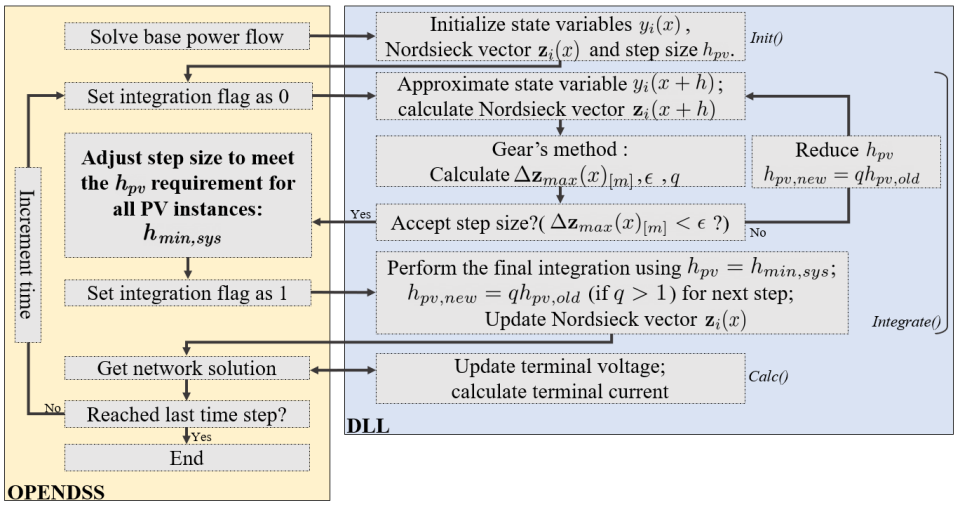

Figure 4.2: Integrative Simulation Framework of OpenDSS and DLL in Dynamic Mode

4.2.1 Nordsieck's formulation

The inverter-based PV system can be represented by a set of first-order differential equations with n state variables

$$y_i'(x) = f_i(x, y_0(x), y_1(x), ..., y_{n-1}(x)), i = 0, 1, ..., n-1, \tag{4.1}$$

which can be written as

$$y_i'(x) = f_i(x, y_i(x)). \tag{4.2}$$

x indicates the time, $x \in [x_0, x_0 + h]$ for one time interval starting at x_0. y_i represents the i^{th} state variable, f_i is the i^{th} differential equation related to y_i.

Nordsieck's method [58] can be treated as a multi-step integration equivalent which has the following working equations (4.3)-(4.8) for a one-step fourth-degree method with step size h:

$$y_i^{[p]} = y_i(x) + h\{f_i(x, y_i(x)) + a_i(x) + b_i(x) + c_i(x)\} \tag{4.3}$$

$$f_i^{[p]} = f_i(x, y_i(x)) + 2a_i(x) + 3b_i(x) + 4c_i(x) \tag{4.4}$$

$$y_i(x + h) = y_i^{[p]} + hY[f_i(x + h, y_i(x + h)) - f_i^{[p]}] \tag{4.5}$$

$$a_i(x + h) = a_i(x) + 3b_i(x) + 6c_i(x) + A[f_i(x + h, y_i(x + h)) - f_i^{[p]}] \tag{4.6}$$

$$b_i(x + h) = b_i(x) + 4c_i(x) + B[f_i(x + h, y_i(x + h)) - f_i^{[p]}] \tag{4.7}$$

$$c_i(x + h) = c_i(x) + C[f_i(x + h, y_i(x + h)) - f_i^{[p]}] \tag{4.8}$$

The terms $a_i(x)$ - $c_i(x)$ are the components in the Nordsieck vector $\mathbf{z}_i(x)$:

$$\mathbf{z}_i(x) = [y_i(x), h \cdot y_i'(x, y_i(x)), h \cdot a_i(x), h \cdot b_i(x), h \cdot c_i(x)]^T, \tag{4.9}$$

which approximate the higher order derivatives of $y_i(x)$:

$$\begin{aligned} \mathbf{z}_i(x) = [y_i(x), h \cdot y_i'(x, y_i(x)), \frac{h^2}{2!} \cdot y_i''(x, y_i(x)), \\ \frac{h^3}{3!} \cdot y_i'''(x, y_i(x)), \frac{h^4}{4!} \cdot y_i''''(x, y_i(x))]^T. \end{aligned} \tag{4.10}$$

The coefficients A,B,C,Y are determined for optimal numerical stability and minimum truncation error of the method[58]:

$$A = \frac{11}{12} \quad B = \frac{1}{3} \quad C = \frac{1}{24} \quad Y = \frac{251}{720} \tag{4.11}$$

$y_i^{[p]}$ and $f_i^{[p]}$ are the predicted values for the state variable and the first order derivative of it at next time step $x + h$ based on the evaluation of the current time step x (4.3),(4.4), the predicted values are first calculated at each time step. The implicit function (4.5) is then solved using Newton's method for the state variables $y_i(x + h)$.

4.2.2 Gear's method for step size control

The truncation error e_i for a single step is[59]:

$$e_i = C_{m+1} h^{m+1} y_i^{(m+1)}(x) + O(h^{m+2}), \tag{4.12}$$

where C_{m+1} depends on the integration method. m is the degree of the integration method, which is 4 for the method being used. The higher degree term $O(h^{m+2})$ can be neglected, then the truncation error is proportional to $h^{m+1} y_i^{(m+1)}(x)$.

$$e_i \propto h^{m+1} y_i^{(m+1)}(x) \tag{4.13}$$

The last component $\mathbf{z}_i(x)_{[m]}$ of the Nordsieck vector $\mathbf{z}_i(x)$ is $\frac{h^m}{m!} \cdot y_i^{(m)}$, so the error e_i can be estimated by the backward difference $\Delta \mathbf{z}_i(x)_{[m]}$ of $\mathbf{z}_i(x)_{[m]}$.

Gear's step size control algorithm is based on the error estimation at each time step. So it is critical to carefully choose the error bound ϵ for the numerical stability of the method. The decision of whether to choose a relative ϵ_{abs} or absolute error bound ϵ_{rel} depends on the solution y_i [59]. Here in this algorithm, we used a mixed error bound:

$$\epsilon = (\epsilon_{abs} + \epsilon_{rel} \cdot y_{max})/6 \tag{4.14}$$

y_{max} is the maximum state variable among y_i, $i = 0, 1, ...n-1$. At each time step, the maximum back difference $\Delta \mathbf{z}_{max}(x)_{[m]}$ among

$$\Delta \mathbf{z}_i(x)_{[m]} = \mathbf{z}_i(x+h)_{[m]} - \mathbf{z}_i(x)_{[m]},\ i = 0, 1, ..., n-1, \tag{4.15}$$

is compared to the error bound ϵ, if

$$\Delta \mathbf{z}_{max}(x)_{[m]} < \epsilon, \tag{4.16}$$

the current step size is accepted and increased for the next step, otherwise, decreased, and the current step is repeated.

The advantage of using Nordsieck's equivalent of the multi-step method is that the step size control can be easily realized. When the step size h changes, the j^{th}, $j = 0, 1, ..., m$, component of the Nordsieck vector $\mathbf{z}_i(x)$ only needs to be multiplied by q^j.

$$q = \frac{h_{new}}{h_{old}} = \frac{1}{\sigma}(\frac{\epsilon}{\Delta \mathbf{z}_{max}(x)_{[m]}})^{\frac{1}{m}} \tag{4.17}$$

$\sigma = 1.2$, which is a safety factor that allows for the neglected terms.

4.3 Simulations and Results

A phasor model for the inverter-based PV system is developed in Chapter 3 based on previous work by [61]. The same 0.6-second simulation is conducted using both the fixed-step size framework and the integrative simulation framework in OpenDSS on the same Arizona utility feeder as section 2.3. All 766 PVs in the network are modeled in the same DLL with details for the inverter current loop and the phase-locked loop (PLL). The simulations are conducted on the same over-voltage scenario with maximum PV generation from the historical data.

Fig. 4.3 shows the dynamic results of one selected PV with large voltage deviation in the system. Terminal voltage, active power and reactive power are compared

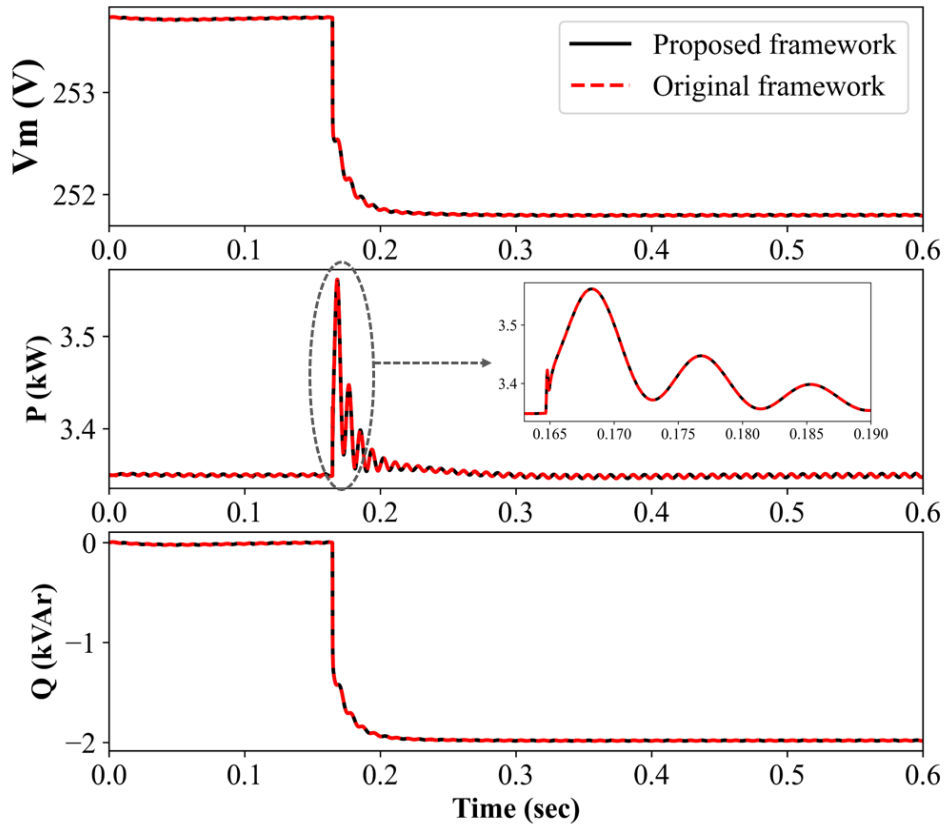

Figure 4.3: Dynamic Results Comparison Between the Original Simulation Framework and the Integrative Framework

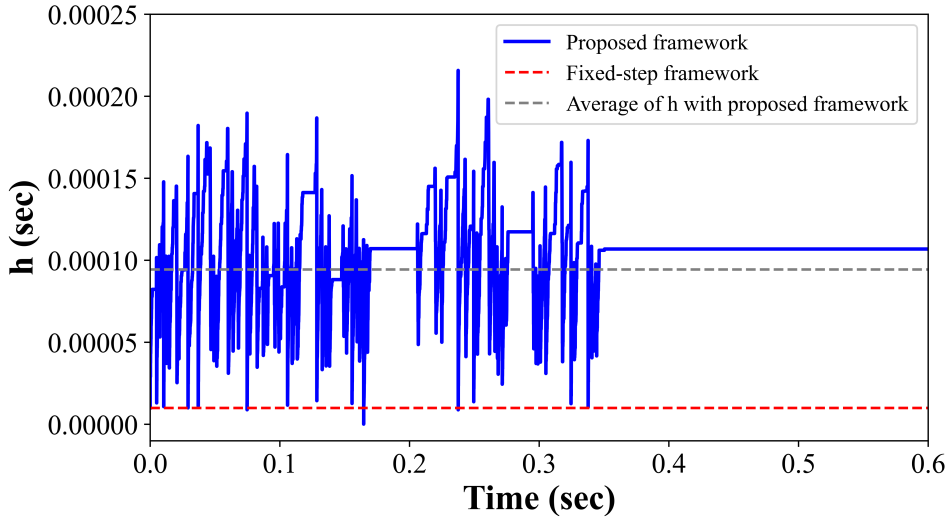

Figure 4.4: Step Size Variation in the Integrative Simulation Framework

between two simulation frameworks. At $t = 0.16s$, the Volt-VAr function is enabled for the 99 PVs in the distribution feeder to ensure the system operates within the acceptable voltage range. The simulation results from the integrative framework match with the embedded framework in OpenDSS, which validates the accuracy of the integrative simulation framework. Fig. 4.4 shows the step size h variation for this particular simulation in the integrative framework. The embedded simulation framework in OpenDSS is set to have a fixed-step size of $1e{-}5$, which is almost the minimum simulation step size allowed by the integrative simulation framework. The average step size for the simulation in the integrative framework is around $9.45e{-}5$. This also indicates the computation time consumption for the simulation in the integrative framework should be less than the original framework in OpenDSS. Table. 4.1 shows the actual time consumed in both simulation frameworks for the 0.6-second simulation, the result proves that the integrative framework can significantly increase the computational efficiency.

Table 4.1: Simulation Time Comparison

Simulation framework	***Fixed-step size***	***Adaptive-step size***
Simulation time (sec)	160	48

4.4 Conclusion

An integrative simulation framework is developed to achieve adaptive-step size dynamic simulation in the distribution system simulator OpenDSS. A Gear-based automatic step size control strategy based on error estimation is applied in the overall adaptive-step size framework. An inverter-based PV phasor model developed in Chapter 3 is used to verify the accuracy and efficiency of the proposed framework in a large-scale actual utility distribution feeder. The results show that the pro-

posed framework can significantly reduce the simulation time for the same simulation compared to the original framework in OpenDSS without sacrificing the simulation accuracy.

One major advantage of this simulation framework is that it allows more complex control functions to be realized in the user-defined DLL without having to set an extremely small step size in the OpenDSS main engine to make the system numerically stable. The inverter-based PV phasor model used in this report is a simple single-phase inverter-based PV model with linear control functions. With the proposed framework, users can write their inverter model with necessary nonlinear control functions or even detailed EMT model with proper phasor extraction technique being implemented.

Chapter 5

CONCLUSIONS AND FUTURE WORK

5.1 Summary

In this research work, the first objective is to develop a long-term planning strategy to optimally upgrade the existing PVs without active voltage control capability in the distribution system to help actively regulate the voltage of the distribution system with high penetration of PV generation. The PV technologies have been evolving for many years with the previous IEEE 1547-2003 standard declaring that the DERs shall not actively regulate the voltage at the point of common coupling (PCC) before the new standard IEEE 1547-2018 was published. Most of the existing PV systems in the real distribution networks are still equipped with the conventional inverters which only allow the PV systems to operate at unity power factor to generate active power. With the upgraded PV inverters, reactive power can be generated or absorbed to maintain the local voltage at the PV system terminals. Since the developed program optimally selects the locations of those upgraded PV among the entire distribution system that has voltage violation issues, the system-wide voltage can be maintained by the PV local voltage control without system-wide communication between different devices. This program provides the utilities with a decision-making tool to help them choose the minimum number of PV inverters to upgrade, which can save their both upgrading and human resource costs. This minimum number of upgraded PV smart inverters is sufficient to mitigate all the voltage violation issues in the distribution system if proper worst-case scenarios are generated for the stochastic programming.

Another concern is that the developed planning tool can not guarantee voltage

stability during the actual operation with active voltage control from the PV inverters. Hence, dynamic studies are also conducted to verify the voltage stability of the studied distribution system. As introduced in section 3.2, for PV inverters with linear control function, the phasor-domain model is sufficient for their dynamic simulation in the distribution system simulator OpenDSS. However, it is necessary to simulate the PV inverter in the time domain when there are nonlinear control functions. A time-domain model for hybrid simulation in OpenDSS is developed, and a PV inverter with nonlinear control functions is tested in this model. This work makes the implementation of complex nonlinear dynamic models possible in OpenDSS.

On the other hand, the high penetration of PV in the distribution system as well as the PV model complexity makes the dynamic simulation less efficient due to the enormous amount of differential equations generated by all the PVs with active control capability. An integrative dynamic simulation framework with adaptive step size control is developed for OpenDSS to conduct dynamic studies in this research work with higher efficiency and without reducing accuracy. One major advantage of this simulation framework is that it allows more complex control functions to be realized in the user-defined dynamic model without having to set an extremely small step size in the OpenDSS main engine to make the system numerically stable.

5.2 Future Work

In this research work, a novel planning strategy to optimally place the PV smart inverter with Volt-VAr control capability has been developed to help regulate the distribution system voltage with minimal costs. However, this optimization strategy does not take the dynamic performance of the PV inverters into account.

Work that needs to be conducted in the future:

- Take different control functions into consideration in the optimization model:

In current research work, only one default set of Q-V curve set points is considered in the Volt-VAr function, which may not be the optimal setting and result in redundant PV smart inverters needed to actively maintain the voltage within the required range. Different set points can be considered in future work. Different grid support functions other than the Volt-VAr control can also be considered in the optimization program.

- Tune the parameter of the PV inverter model with MRAC scheme to get better performance in large-scale systems.
- Improve the integrative simulation tool in OpenDSS

REFERENCES

[1] A. Bedawy, N. Yorino, K. Mahmoud, Y. Zoka, and Y. Sasaki, "Optimal voltage control strategy for voltage regulators in active unbalanced distribution systems using multi-agents," *IEEE Transactions on Power Systems*, vol. 35, no. 2, pp. 1023–1035, 2020.

[2] K. E. Antoniadou-Plytaria, I. N. Kouveliotis-Lysikatos, P. S. Georgilakis, and N. D. Hatziargyriou, "Distributed and decentralized voltage control of smart distribution networks: Models, methods, and future research," *IEEE Transactions on Smart Grid*, vol. 8, no. 6, pp. 2999–3008, 2017.

[3] A. Keane, L. F. Ochoa, C. L. T. Borges, G. W. Ault, A. D. Alarcon-Rodriguez, R. A. F. Currie, F. Pilo, C. Dent, and G. P. Harrison, "State-of-the-art techniques and challenges ahead for distributed generation planning and optimization," *IEEE Transactions on Power Systems*, vol. 28, no. 2, pp. 1493–1502, 2013.

[4] "IEEE standard for interconnection and interoperability of distributed energy resources with associated electric power systems interfaces," *IEEE Std 1547-2018 (Revision of IEEE Std 1547-2003)*, pp. 1–138, 2018.

[5] "Ieee standard for interconnecting distributed resources with electric power systems," *IEEE Std 1547-2003*, pp. 1–28, 2003.

[6] T. E. McDermott, "Modeling pv for unbalanced, dynamic and quasistatic distribution system analysis," in *2011 IEEE Power and Energy Society General Meeting*, 2011, pp. 1–3.

[7] V. Jalili-Marandi, V. Dinavahi, K. Strunz, J. A. Martinez, and A. Ramirez, "Interfacing techniques for transient stability and electromagnetic transient programs ieee task force on interfacing techniques for simulation tools," *IEEE Transactions on Power Delivery*, vol. 24, no. 4, pp. 2385–2395, 2009.

[8] H. Sun, Q. Guo, J. Qi, V. Ajjarapu, R. Bravo, J. Chow, Z. Li, R. Moghe, E. Nasr-Azadani, U. Tamrakar, G. N. Taranto, R. Tonkoski, G. Valverde, Q. Wu, and G. Yang, "Review of challenges and research opportunities for voltage control in smart grids," *IEEE Transactions on Power Systems*, vol. 34, no. 4, pp. 2790–2801, 2019.

[9] H. Zhu and H. J. Liu, "Fast local voltage control under limited reactive power: Optimality and stability analysis," *IEEE Transactions on Power Systems*, vol. 31, no. 5, pp. 3794–3803, 2016.

[10] R. Tonkoski, L. A. C. Lopes, and T. H. M. El-Fouly, "Coordinated active power curtailment of grid connected pv inverters for overvoltage prevention," *IEEE Transactions on Sustainable Energy*, vol. 2, no. 2, pp. 139–147, 2011.

[11] S. Alyami, Y. Wang, C. Wang, J. Zhao, and B. Zhao, "Adaptive real power capping method for fair overvoltage regulation of distribution networks with high penetration of pv systems," *IEEE Transactions on Smart Grid*, vol. 5, no. 6, pp. 2729–2738, 2014.

[12] K. Baker, A. Bernstein, E. Dall'Anese, and C. Zhao, "Network-cognizant voltage droop control for distribution grids," *IEEE Transactions on Power Systems*, vol. 33, no. 2, pp. 2098–2108, 2018.

[13] A. Dutta, S. Ganguly, and C. Kumar, "Model predictive control based coordinated voltage control in active distribution networks utilizing oltc and dstatcom," in *2020 IEEE International Conference on Power Electronics, Drives and Energy Systems (PEDES)*, 2020, pp. 1–6.

[14] M. Juamperez, G. Yang, and S. B. Kjær, "Voltage regulation in lv grids by coordinated volt-var control strategies," *Journal of Modern Power Systems and Clean Energy*, vol. 2, no. 4, pp. 319–328, 2014.

[15] K. M. Rogers, R. Klump, H. Khurana, A. A. Aquino-Lugo, and T. J. Overbye, "An authenticated control framework for distributed voltage support on the smart grid," *IEEE Transactions on Smart Grid*, vol. 1, no. 1, pp. 40–47, 2010.

[16] A. Kulmala, S. Repo, and P. Järventausta, "Coordinated voltage control in distribution networks including several distributed energy resources," *IEEE Transactions on Smart Grid*, vol. 5, no. 4, pp. 2010–2020, 2014.

[17] B. A. Robbins, C. N. Hadjicostis, and A. D. Domínguez-García, "A two-stage distributed architecture for voltage control in power distribution systems," *IEEE Transactions on Power Systems*, vol. 28, no. 2, pp. 1470–1482, 2013.

[18] H. Gao, J. Liu, L. Wang, and Z. Wei, "Decentralized energy management for networked microgrids in future distribution systems," *IEEE Transactions on Power Systems*, vol. 33, no. 4, pp. 3599–3610, 2018.

[19] M. Asano, A. Hirayama, F. Wong, R. Moghe, H. Chun, and D. Tholomier, "Application of dynamic v ar controllers for increasing solar hosting capacity in distribution grids," in *2020 IEEE/PES Transmission and Distribution Conference and Exposition (T D)*, 2020, pp. 1–5.

[20] X. Ye, Q. Tang, T. Li, X. Tong, O. YANG, F. Wen, and H. Li, "Planning for energy storage system considering risk of inflexibility in active distribution network," in *2019 IEEE 3rd International Electrical and Energy Conference (CIEEC)*, 2019, pp. 259–263.

[21] X. Qian, S. Zhang, J. Liu, Y. Zheng, and W. Liu, "Hierarchical optimal planning of battery energy storage systems in radial distribution networks," in *2019 IEEE 3rd Conference on Energy Internet and Energy System Integration (EI2)*, 2019, pp. 84–89.

[22] J. B. Noshahr, B. Mohamadi, M. Kermani, and M. Kermani, "Operational planning of inverter control in a grid connected microgrid with hybrid pv and bess," in *2020 IEEE International Conference on Environment and Electrical Engineering and 2020 IEEE Industrial and Commercial Power Systems Europe (EEEIC / I CPS Europe)*, 2020, pp. 1–5.

[23] S. Sannigrahi, S. R. Ghatak, and P. Acharjee, "Coordinated planning of distribution system with res, dstatcom, and protective devices," *IEEE Transactions on Industry Applications*, vol. 57, no. 4, pp. 4294–4305, 2021.

[24] Y. Niazi, M. E. H. Golshan, and H. H. Alhelou, "Combined firm and renewable distributed generation and reactive power planning," *IEEE Access*, vol. 9, pp. 133 735–133 745, 2021.

[25] S. Conti and A. M. Greco, "Active mv distribution network planning coordinated with advanced centralized voltage regulation system," in *2007 IEEE Lausanne Power Tech*, 2007, pp. 2105–2109.

[26] W. Liu, H. Xu, and S. Niu, "An integrated planning method of active distribution system considering decentralized voltage control," in *2016 IEEE Power and Energy Society General Meeting (PESGM)*, 2016, pp. 1–5.

[27] Y. Xu, Z. Y. Dong, R. Zhang, and D. J. Hill, "Multi-timescale coordinated voltage/var control of high renewable-penetrated distribution systems," *IEEE Transactions on Power Systems*, vol. 32, no. 6, pp. 4398–4408, 2017.

[28] S. Singh, S. Veda, S. P. Singh, R. Jain, and M. Baggu, "Event-driven predictive approach for real-time volt/var control with cvr in solar pv rich active distribution network," in *2022 IEEE Power and Energy Society General Meeting (PESGM)*, 2022, pp. 1–1.

[29] X. Sun and J. Qiu, "Two-stage volt/var control in active distribution networks with multi-agent deep reinforcement learning method," *IEEE Transactions on Smart Grid*, vol. 12, no. 4, pp. 2903–2912, 2021.

[30] Y. Long and D. S. Kirschen, "Bi-level volt/var optimization in distribution networks with smart pv inverters," *IEEE Transactions on Power Systems*, vol. 37, no. 5, pp. 3604–3613, 2022.

[31] R. Xu, C. Zhang, Y. Xu, Z. Dong, and R. Zhang, "Multi-objective hierarchically-coordinated volt/var control for active distribution networks with droop-controlled pv inverters," *IEEE Transactions on Smart Grid*, vol. 13, no. 2, pp. 998–1011, 2022.

[32] C. Zhang, Y. Xu, Y. Wang, Z. Y. Dong, and R. Zhang, "Three-stage hierarchically-coordinated voltage/var control based on pv inverters considering distribution network voltage stability," *IEEE Transactions on Sustainable Energy*, vol. 13, no. 2, pp. 868–881, 2022.

[33] S. Karagiannopoulos, P. Aristidou, and G. Hug, "Hybrid approach for planning and operating active distribution grids," *IET Generation, Transmission & Distribution*, vol. 11, 10 2016.

[34] S. Karagiannopoulos, P. Aristidou, and G. Hug, "Co-optimisation of planning and operation for active distribution grids," in *2017 IEEE Manchester PowerTech*, 2017, pp. 1–6.

[35] Impact of Inverter Based Generation on Bulk Power System Dynamics and Short-Circuit Performance, IEEE PES Industry Technical Support Task Force, PES-TR68, 2018. [Online]. Available: https://resourcecenter.ieee-pes.org/publications/technical-reports/PES_TR_7-18_0068.html.

[36] X. Mao and R. Ayyanar, "Average and phasor models of single phase pv generators for analysis and simulation of large power distribution systems," in *2009 Twenty-Fourth Annual IEEE Applied Power Electronics Conference and Exposition*, 2009, pp. 1964–1970.

[37] W. Du, F. K. Tuffner, K. P. Schneider, R. H. Lasseter, J. Xie, Z. Chen, and B. Bhattarai, "Modeling of grid-forming and grid-following inverters for dynamic simulation of large-scale distribution systems," *IEEE Transactions on Power Delivery*, vol. 36, no. 4, pp. 2035–2045, 2021.

[38] M. M. Koutenaei, T.-T. Nguyen, T. Vu, S. Paudyal, and R. Hovsapian, "Efficient phasor-based dynamic volt/var and volt/watt analysis of large distribution grid with high penetration of smart inverters," *IEEE Transactions on Smart Grid*, vol. 13, no. 5, pp. 3997–4008, 2022.

[39] X. Mao and R. Ayyanar, "An adaptive controller for inverter-interfaced dgs connected to grids with a wide range of unknown impedances," in *2010 IEEE Energy Conversion Congress and Exposition*, 2010, pp. 2871–2877.

[40] G. Liu, X. Cao, T. Shi, and W. Wang, "Research on adaptive control of grid-connected pv inverters in weak grid," in *2015 IEEE Energy Conversion Congress and Exposition (ECCE)*, 2015, pp. 4229–4235.

[41] F. Plumier, P. Aristidou, C. Geuzaine, and T. Van Cutsem, "Co-simulation of electromagnetic transients and phasor models: A relaxation approach," *IEEE Transactions on Power Delivery*, vol. 31, no. 5, pp. 2360–2369, 2016.

[42] A. Hariri and M. O. Faruque, "A hybrid simulation tool for the study of pv integration impacts on distribution networks," *IEEE Transactions on Sustainable Energy*, vol. 8, no. 2, pp. 648–657, 2017.

[43] D. Shu, X. Xie, Q. Jiang, Q. Huang, and C. Zhang, "A novel interfacing technique for distributed hybrid simulations combining emt and transient stability models," *IEEE Transactions on Power Delivery*, vol. 33, no. 1, pp. 130–140, 2018.

[44] Q. Huang and V. Vittal, "Advanced emt and phasor-domain hybrid simulation with simulation mode switching capability for transmission and distribution systems," *IEEE Transactions on Power Systems*, vol. 33, no. 6, pp. 6298–6308, 2018.

[45] K. Prabakar, B. Palmintier, A. Pratt, A. Hariri, I. Mendoza, and M. Baggu, "Improving the performance of integrated power-hardware-in-the-loop and quasi-static time-series simulations," *IEEE Transactions on Industrial Electronics*, vol. 68, no. 11, pp. 10 938–10 948, 2021.

[46] C. Scheibe, A. Kuri, L. Graf, R. Venugopal, and G. Mehlmann, "Real time co-simulation of electromechanical and electromagnetic power system models," in *2022 International Conference on Smart Energy Systems and Technologies (SEST)*, 2022, pp. 1–6.

[47] X. Sun, J. Qiu, and J. Zhao, "Real-time volt/var control in active distribution networks with data-driven partition method," *IEEE Transactions on Power Systems*, vol. 36, no. 3, pp. 2448–2461, 2021.

[48] Z. Soltani, S. Ma, M. Khorsand, and V. Vittal, "Simultaneous robust state estimation, topology error processing, and outage detection for unbalanced distribution systems," *IEEE Transactions on Power Systems*, pp. 1–15, 2022.

[49] B. A. Robbins and A. D. Domínguez-García, "Optimal reactive power dispatch for voltage regulation in unbalanced distribution systems," *IEEE Transactions on Power Systems*, vol. 31, no. 4, pp. 2903–2913, 2016.

[50] Q. Zhang, K. Dehghanpour, and Z. Wang, "Distributed cvr in unbalanced distribution systems with pv penetration," *IEEE Transactions on Smart Grid*, vol. 10, no. 5, pp. 5308–5319, 2019.

[51] Z. Yu, Y. Tang, T. Yao, and R. Ayyanar, "Dynamic simulation of cig in large unbalanced distribution systems using an open source tool," *IET Generation Transmission & Distribution*, vol. 13, pp. 1638–1645, 2019.

[52] OpenDSS, EPRI Distribution System Simulator, [Online]. Available: https://sourceforge.net/projects/electricdss/.

[53] GridLAB-D, A Unique Tool to Design the Smart Grid, [Online]. Available: https://www.gridlabd.org.

[54] CYME, Power Engineering Software, [Online]. Available: http://www.cyme.com/software/cymdist/.

[55] J. Peppanen, J. Taylor, D. Fonseca, J. Snodgrass, S. Chen, and T. I. Strasser, "Distributed energy resource benchmark models for distribution impact assessment - update of activities by cigre working group c6.36," in *CIRED 2021 - The 26th International Conference and Exhibition on Electricity Distribution*, vol. 2021, 2021, pp. 1988–1992.

[56] R. C. Dugan and D. Montenegro, "Reference Guide: The open distribution system simulator (OpenDSS)," EPRI, Tech. Rep., May. 2022.

[57] A. Nagarajan and R. Ayyanar, "Dynamic analysis of distribution systems with high penetration of pv generators using differential algebraic equations in opendss," in *2014 North American Power Symposium (NAPS)*, 2014, pp. 1–6.

[58] A. Nordsieck, "On numerical integration of ordinary differential equations," *Mathematics of Computation*, vol. 16, no. 77, pp. 22–49, 1962.

[59] C. W. Gear, "The automatic integration of ordinary differential equations," *Communications of the ACM*, vol. 14, no. 3, pp. 176–179, 1971.

[60] J. P. Moreau, "Jean-pierre moreau's home page." [Online]. Available: http://http://jean-pierre.moreau.pagesperso-orange.fr

[61] Z. Yu, Y. Tang, T. Yao, and R. Ayyanar, "Dynamic simulation of cig in large unbalanced distribution systems using an open source tool," *Iet Generation Transmission & Distribution*, vol. 13, pp. 1638–1645, 2019.